

Does thermal leptogenesis in a canonical seesaw rely on initial memory?

Partha Kumar Paul^{1,*}, Narendra Sahu^{1,†} and Shashwat Sharma^{1,‡}

¹*Department of Physics, Indian Institute of Technology Hyderabad, Kandi, Sangareddy, Telangana-502285, India.*

(Dated: May 7, 2026)

It is a common lore that in thermal leptogenesis within the type-I seesaw framework and a hierarchical spectrum of heavy right-handed neutrinos (RHNs), the CP-violating, out-of-equilibrium decay of the lightest RHN (N_1) is the only relevant source of the final $B - L$ asymmetry, since any asymmetry produced by the heavier RHNs is expected to be erased by subsequent N_1 -mediated washout processes. In this work, we revisit this assumption by solving the density-matrix equations, including decay, inverse decay, and relevant scattering processes, and by fully accounting for flavor-projection effects induced by the Yukawa coupling structure. We show that the asymmetries generated by the heavier RHNs (N_2 and N_3) generally possess components that are misaligned in flavor space with respect to N_1 , resulting in a partially protected contribution that survives the N_1 washout. Unlike the conventional picture of N_2 -dominated leptogenesis, this memory effect arises even when N_1 remains dynamically relevant and cannot be captured within the classical Boltzmann framework. Furthermore, imposing consistency with low-energy neutrino mass and mixing data, we find that at most one RHN can lie in the weak washout regime, which naturally divides the parameter space into four distinct dynamical regimes. We systematically quantify the memory effect in each regime and demonstrate that it can significantly modify the final $B - L$ asymmetry. We find that including projection effects can indeed extend the viable parameter space into the sensitivity range of neutrinoless double beta decay experiments.

I. INTRODUCTION

One of the most profound mysteries in cosmology is the observed baryon asymmetry of the Universe, which is the imbalance between matter and antimatter. The early Universe should have created equal amounts of matter and antimatter, but observations show that matter dominated over antimatter. This asymmetry is quantified as the baryon-to-photon ratio: $\eta_B = \frac{n_B - n_{\bar{B}}}{n_\gamma} = (6.14 \pm 0.04) \times 10^{-10}$ as determined by the cosmic microwave background [1] and the big bang nucleosynthesis [2–5]. The standard model (SM) of particle physics cannot account for this observed imbalance between matter and antimatter.

Thermal leptogenesis in a canonical seesaw provides a simple yet compelling mechanism for explaining the observed baryon asymmetry of the Universe [6–15]. It connects the matter-antimatter asymmetry with the origin of non-zero neutrino mass as revealed by oscillation experiments [16–21] via the type-I seesaw framework [22–27]. This mechanism is based on the CP violating out-of-equilibrium decay of heavy right-handed neutrinos (RHNs) to SM leptons and Higgs, producing a net lepton asymmetry which finally gets converted to the baryon asymmetry via the electroweak (EW) sphalerons [28, 29]. A common assumption in this framework is that the lightest RHN, N_1 is the primary contributor to the final $B - L$ asymmetry, as any asymmetries generated by the decays of heavier RHNs (N_2, N_3) are presumed to be

erased by the lepton number violating processes mediated by N_1 [11]. This assumption simplifies the analysis of thermal leptogenesis, effectively decoupling the dynamics of N_1 from N_2 and N_3 . However, as we delineate in this paper, the validity of this assumption is not always correct.

In this paper, we revisit the validity of this assumption by considering four different cases. We saw that, to satisfy the neutrino masses and mixing given by the low-energy neutrino oscillation data, at most one of the RHNs can be in the weak washout regime. Therefore, the four different cases can be: I) All the RHNs are in the strong washout regime, II) N_1 is in the weak washout regime while N_2 and N_3 are in the strong washout regime, III) N_2 is in the weak washout regime while N_1 and N_3 are in the strong washout regime, and finally IV) N_3 is in the weak washout regime while N_1 and N_2 are in the strong washout regime. In all the above four cases, we use the density matrix formalism to demonstrate the percentage survival of the pre-existing asymmetries produced by the heavier RHNs.

We assume that thermal leptogenesis occurs at temperatures $T \gtrsim 10^{12}$ GeV, where the charged-lepton Yukawa interactions are out of equilibrium. In this regime, the lepton doublets produced in the decays of RHNs are usually assumed to be indistinguishable, and hence all generated asymmetries are considered to be aligned in flavor space [30]. This leads to a complete erasure of the pre-existing asymmetries produced by N_2 and N_3 via lepton number-violating processes mediated by N_1 . However, this assumption of perfect alignment among the asymmetries produced by different RHNs is not generally true and strongly depends on the Yukawa coupling texture. In reality, the lepton states produced by the decays of distinct RHNs need not be identical—each RHN cou-

* ph22resch11012@iith.ac.in

† nsahu@phy.iith.ac.in

‡ ph23resch11016@iith.ac.in

ples to a different linear combination of lepton flavors ($|l_i\rangle = \sum_\alpha \mathcal{C}_{i\alpha} |l_\alpha\rangle$ where $\alpha = e, \mu, \tau$) [12, 31–40]. Consequently, the asymmetries generated by N_2 and N_3 can have components that are orthogonal to the direction of N_1 -decay and are not erased by the lepton number violating interactions of N_1 , while those parallel to the direction of N_1 -decay can be erased. This leads to a protected portion of the asymmetries generated by $N_{2,3}$ that survive and contribute to the final $B - L$ asymmetry. We refer to the percentage survival of the pre-existing asymmetry as “*memory effect*”. Such effects cannot be captured within the classical Boltzmann approach, which tracks only the total lepton number density. To consistently describe the evolution of coherence among different heavy-neutrino flavor states and the corresponding asymmetries, we use the density matrix formalism. We solve the density matrix equation for the four washout regimes discussed in the previous paragraph and delineate the memory effect in all cases.

The paper is organized as follows. In section II, we briefly recapitulate the type-I seesaw mechanism, while in section III, we show the details of the density matrix formalism for leptogenesis. We discuss the results in section IV by comparing the memory effect (δ) with respect to the mass ratios (M_2/M_1 and M_3/M_1), considering decays, inverse decays, and scatterings. We compare the numerical solution of the full density matrix equations with the analytical approximation in section V. In section VI, we discuss the importance of projection effects in neutrinoless double beta decay. We finally conclude in section VII by summarizing our results and discussing the impact of heavier RHNs (N_2 and N_3) on the final $B - L$ asymmetry.

II. TYPE-I SEESAW

In the canonical type-I seesaw, the SM is extended with three RHNs, N_1, N_2, N_3 , which are singlets under the SM gauge group ($SU(3)_C \times SU(2)_L \times U(1)_Y$). The Lagrangian responsible for generating lepton asymmetry as well as neutrino mass is given as¹

$$-\mathcal{L}^{\text{type-I}} \supset \frac{1}{2} M_R \bar{N}^c N + Y \bar{l} \tilde{H} N + \text{H.c.} \quad (1)$$

Here, $\tilde{H} = i\sigma_2 H^*$ where H is the Higgs doublet and $l = \begin{pmatrix} \nu_L \\ l_L \end{pmatrix}$ is the lepton doublet. From Eq.(1) we can write the 6×6 neutral fermion mass matrix as

$$\begin{pmatrix} \bar{\nu}_L^c & \bar{N}_R \end{pmatrix} \begin{pmatrix} m_L & m_D \\ m_D^T & M_R \end{pmatrix} \begin{pmatrix} \nu_L \\ N_R^c \end{pmatrix} + \text{H.c.} \quad (2)$$

where $m_D = \frac{Yv}{\sqrt{2}}$ (v is the Higgs vacuum expectation value (vev)). Thus, for $M_R \gg vY/\sqrt{2}$, we can write

$$m_\nu = -m_D M_R^{-1} m_D^T = -\frac{v^2}{2} Y M_R^{-1} Y^T. \quad (3)$$

Thus, the large RHN masses give an origin to the tiny masses of the active neutrinos via the type-I seesaw mechanism. The light neutrino mass matrix (m_ν) can be diagonalized using the unitary Pontecorvo–Maki–Nakagawa–Sakata (PMNS) matrix U

$$D_m = U^T m_\nu U, \quad (4)$$

where $D_m = \text{diag}(m_1, m_2, m_3)$. Using Eq.(3) in Eq.(4), we get

$$D_m = -\frac{v^2}{2} U^T Y M_R^{-1} Y^T U. \quad (5)$$

Without loss of generality, we assume the heavy RHNs to be in a diagonal mass basis. We then denote $M_R = D_M = \text{diag}(M_1, M_2, M_3)$, thus from Eq.(5) we can write

$$-\frac{v^2}{2} (D_{\sqrt{m^{-1}}} U^T Y D_{\sqrt{M^{-1}}}) (D_{\sqrt{m^{-1}}} Y^T U D_{\sqrt{m^{-1}}}) = I_{3 \times 3}. \quad (6)$$

Here, the notation $D_{\sqrt{A}}$ means $\sqrt{D_A}$. Since, $(D_{\sqrt{M^{-1}}} Y^T U D_{\sqrt{m^{-1}}})^T = (D_{\sqrt{m^{-1}}} U^T Y D_{\sqrt{M^{-1}}})$, we can write

$$-\frac{iv}{\sqrt{2}} (D_{\sqrt{m^{-1}}} U^T Y D_{\sqrt{M^{-1}}}) = R^T, \quad (7)$$

where, R is a complex orthogonal matrix with $R^T R = I$. Thus, using Eq.(7), we can write the Yukawa coupling matrix as

$$Y = \frac{i\sqrt{2}}{v} U^* D_{\sqrt{m}} R^T D_{\sqrt{M}}. \quad (8)$$

This is known as the Casas-Ibarra Parameterization of the Yukawa coupling matrix [41]. This implies that larger values of RHNs’ masses lead to larger Yukawa couplings, holding all other parameters fixed. The PMNS matrix U is given by [3]

$$U = \begin{pmatrix} c_{12}c_{13} & s_{12}c_{13} & s_{13}e^{-i\delta} \\ -s_{12}c_{23} - c_{12}s_{13}s_{23}e^{i\delta} & c_{12}c_{23} - s_{12}s_{13}s_{23}e^{i\delta} & c_{13}s_{23} \\ s_{12}s_{23} - c_{12}s_{13}c_{23}e^{i\delta} & -c_{12}s_{23} - s_{12}s_{13}c_{23}e^{i\delta} & c_{13}c_{23} \end{pmatrix} \cdot \begin{pmatrix} e^{i\eta_1} & 0 & 0 \\ 0 & e^{i\eta_2} & 0 \\ 0 & 0 & 1 \end{pmatrix}, \quad (9)$$

where $c_{ij} = \cos \theta_{ij}$ and $s_{ij} = \sin \theta_{ij}$ and δ is the Dirac CP phase and $\eta_{1,2}$ are the Majorana CP phases. We randomly choose Majorana phases in the range $(0, 2\pi)$ and take the neutrino oscillation parameters to be in the 3σ range [42]. We also consider the mass of the lightest SM neutrino (m_1) to be zero. In the general case, the

¹ We have suppressed the generation indices.

complex orthogonal matrix R in Eq.(8) can be described by 3 different complex angles ($\theta_i = x_i + iy_i; i = 1, 2, 3$) with a form of

$$R = \begin{pmatrix} \cos \theta_1 & -\sin \theta_1 & 0 \\ \sin \theta_1 & \cos \theta_1 & 0 \\ 0 & 0 & 1 \end{pmatrix} \begin{pmatrix} \cos \theta_2 & 0 & \sin \theta_2 \\ 0 & 1 & 0 \\ -\sin \theta_2 & 0 & \cos \theta_2 \end{pmatrix} \begin{pmatrix} 1 & 0 & 0 \\ 0 & \cos \theta_3 & -\sin \theta_3 \\ 0 & \sin \theta_3 & \cos \theta_3 \end{pmatrix} \quad (10)$$

Thus given, $\theta_1, \theta_2, \theta_3, M_1, M_2, M_3$, one can derive a Yukawa coupling matrix using Eq.(8).

III. DENSITY MATRIX FORMALISM FOR SEQUENTIAL LEPTOGENESIS IN TYPE-I SEESAW

In the type-I seesaw, the Majorana nature of the heavy RHNs naturally leads to lepton number violation. In an expanding universe, the CP -violating, out-of-equilibrium decays of the heavy RHNs can give rise to the lepton asymmetry [6–12]. The interference between the tree-level and one-loop decay diagrams (self-energy correction and vertex term) gives the required CP asymmetry, as shown in Fig. 1.

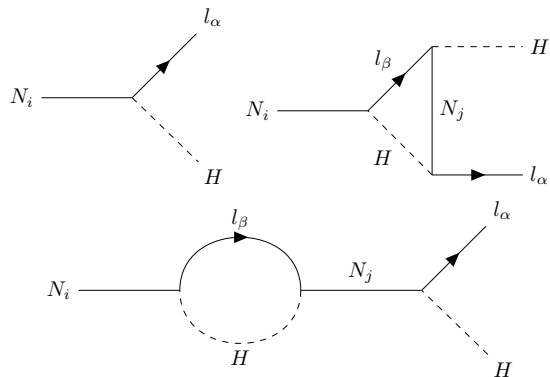


FIG. 1. Tree and one-loop level decays of RHNs giving rise to nonzero CP asymmetry.

The CP asymmetry parameter is defined as

$$\varepsilon_i = \frac{\Gamma(N_i \rightarrow lH) - \Gamma(N_i \rightarrow \bar{l}\bar{H})}{\Gamma(N_i \rightarrow lH) + \Gamma(N_i \rightarrow \bar{l}\bar{H})} \quad (11)$$

Considering the interference of tree-level diagrams with one-loop diagrams, we have [43]

$$\varepsilon_i = -\frac{1}{8\pi} \sum_{j \neq i} \frac{\text{Im}[(Y^\dagger Y)_{ij}^2]}{(Y^\dagger Y)_{ii}} \left[f_v \left(\frac{M_j^2}{M_i^2} \right) + f_s \left(\frac{M_j^2}{M_i^2} \right) \right] \quad (12)$$

where $f_v(x)$ comes from the one-loop vertex term and $f_s(x)$ comes from the one-loop self-energy term, and they

are given by

$$f_s(x) = \frac{\sqrt{x}}{1-x};$$

$$f_v(x) = \sqrt{x} \left[1 - (1+x) \ln \left(\frac{1+x}{x} \right) \right]. \quad (13)$$

In standard (semi-classical) Boltzmann equations, we track the number densities of heavy neutrinos N_i and the lepton doublets l_α ($\alpha = e, \mu, \tau$). At very high temperatures ($T \gtrsim 10^{12} \text{GeV}$), the charged-lepton Yukawa interactions are out-of-equilibrium, so all lepton flavors behave coherently, which is the flavor blind regime. If the heavy Majorana neutrino N_i decays into a lepton/anti-lepton doublet at a temperature $T \gtrsim 10^{12} \text{GeV}$, the produced lepton/anti-lepton doublet $|l_i\rangle$ is a coherent superposition of the lepton flavor states $|l_\alpha\rangle$ given by ²

$$|l_i\rangle = \sum_{\alpha} c_{i\alpha} |l_\alpha\rangle, \quad c_{i\alpha} = \langle l_\alpha | l_i \rangle,$$

$$|\bar{l}_i\rangle = \sum_{\alpha} \bar{c}_{i\alpha} |\bar{l}_\alpha\rangle, \quad \bar{c}_{i\alpha} = \langle \bar{l}_\alpha | \bar{l}_i \rangle \quad (14)$$

where the coefficients $c_{i\alpha}$ are determined by the Yukawa couplings $Y_{i\alpha}$ as $c_{i\alpha} = \frac{Y_{i\alpha}}{\sqrt{(Y^\dagger Y)_{ii}}}$, which satisfy $\sum_{\alpha} |c_{i\alpha}|^2 = 1$.

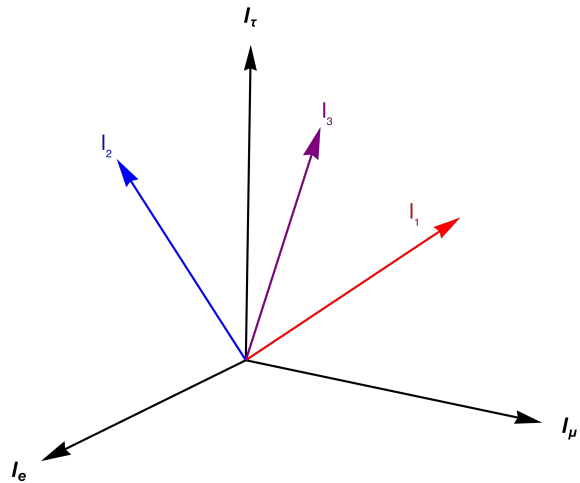


FIG. 2. Figure illustrating the produced lepton l_i from N_i decays as “flavor vector” in the flavor space.

Given that these “vectors” have different coefficients, they are in general not parallel to each other in the flavor space, which is illustrated in Fig.2. Since they have some arbitrary alignment defined by the Yukawa coupling texture, it is allowed that l_i has some component which is orthogonal to l_j and is thus protected from inverse decay

² Without loss of generality we take $|l_\alpha\rangle$ ($\alpha = e, \mu, \tau$) to be an orthogonal basis.

washout effects of l_j . This is called the projection effect. In this paper, we consider the asymmetry produced by all three RHNs by taking into account the projection effects and compare our result with the asymmetry produced by N_1 decay only. Since l_i are vectors in the flavor space, we can define 3 different orthogonal bases: $(l_i, l_i^{\perp(1)}, l_i^{\perp(2)})$ where $i = 1, 2, 3$ as shown in Fig.3. We conveniently refer to them as ‘‘RHN flavor basis’’ because N_i are allowed to decay along the l_i directions and are expressed as

$$\begin{aligned} |l_i\rangle &= c_{i\tau} |l_\tau\rangle + c_{i\mu} |l_\mu\rangle + c_{ie} |l_e\rangle \\ |l_i^{\perp(1)}\rangle &= \frac{0 |l_\tau\rangle + c_{ie}^* |l_\mu\rangle - c_{i\mu}^* |l_e\rangle}{\sqrt{|c_{ie}|^2 + |c_{i\mu}|^2}} \\ |l_i^{\perp(2)}\rangle &= \frac{(1 - |c_{i\tau}|^2) |l_\tau\rangle - c_{i\mu} c_{i\tau}^* |l_\mu\rangle - c_{ie} c_{i\tau}^* |l_e\rangle}{\sqrt{|c_{ie}|^2 + |c_{i\mu}|^2}} \end{aligned} \quad (15)$$

Here, any asymmetry produced in the direction $l_i^{\perp,1,2}$ is protected from the washout effects in the l_i direction (say for instance $l_i H \rightarrow N_i$).

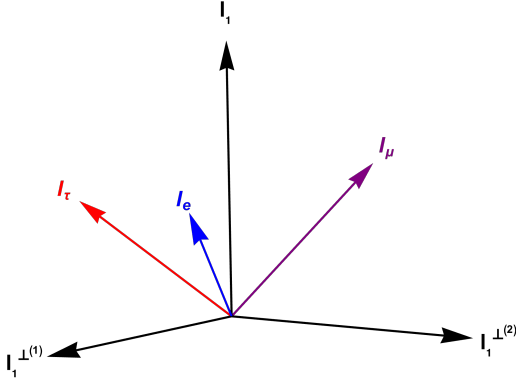


FIG. 3. Figure illustrating the new basis $(l_i, l_i^{\perp(1)}, l_i^{\perp(2)})$ defined in the flavor space.

Now, for the production of l_i from $N_i \rightarrow l_i H$ interaction, we can define a matrix $\mathcal{P}^{(i)} = \text{diag}(1, 0, 0)$ in the respective basis $(l_i, l_i^{\perp(1)}, l_i^{\perp(2)})$ where $i = 1, 2, 3$, called the projection matrix. Since the projection matrices are defined in the RHN flavor basis, we can use Eq.(15) to define a similarity transformation to represent the projection matrix in the charged flavor basis or in a different RHN flavor basis, which is shown as

$$\mathcal{P}_{i_I j_I}^{(I)} = R_{i_I \alpha}^{(I)\dagger} R_{\beta i_J}^{(J)} \mathcal{P}_{i_J j_J}^{(J)} R_{j_J \beta}^{(J)\dagger} R_{\beta j_I}^{(I)} \quad (16)$$

where I, J represents the RHN generation (1, 2, 3), α, β denotes the charged flavors (e, μ, τ) and i_I, j_I represents the element location in the matrix corresponding to the I^{th} RHN generation. Using Eq.(15), the matrix R^I is

given by

$$R^I = \begin{pmatrix} c_{I\tau} \frac{1 - |c_{I\tau}|^2}{\sqrt{|c_{Ie}|^2 + |c_{I\mu}|^2}} & 0 \\ c_{I\mu} \frac{-c_{I\mu} c_{I\tau}^*}{\sqrt{|c_{Ie}|^2 + |c_{I\mu}|^2}} & \frac{c_{Ie}^*}{\sqrt{|c_{Ie}|^2 + |c_{I\mu}|^2}} \\ c_{Ie} \frac{-c_{Ie} c_{I\tau}^*}{\sqrt{|c_{Ie}|^2 + |c_{I\mu}|^2}} & \frac{-c_{I\mu}^*}{\sqrt{|c_{Ie}|^2 + |c_{I\mu}|^2}} \end{pmatrix} \quad (17)$$

Now, using Eq.(16), and 17, we can define all the projection matrices $\mathcal{P}^{(I)}$ in the RHN flavor basis $(l_1, l_1^{\perp(1)}, l_1^{\perp(2)})$. In this basis, the density matrix equations are given as

$$\begin{aligned} \frac{dN_{N_1}}{dz} &= -(D_1 + S_1)(N_{N_1} - N_{N_1}^{eq}), \\ \frac{dN_{N_2}}{dz} &= -(D_2 + S_2)(N_{N_2} - N_{N_2}^{eq}), \\ \frac{dN_{N_3}}{dz} &= -(D_3 + S_3)(N_{N_3} - N_{N_3}^{eq}), \\ \frac{dN_{ij}^{B-L}}{dz} &= \sum_{k=1}^3 \left(-\varepsilon_{ij}^{(k)} D_k (N_{N_k} - N_{N_k}^{eq}) - \frac{1}{2} W_k \{ \mathcal{P}^{(k)}, N^{B-L} \}_{ij} \right) \end{aligned} \quad (18)$$

where, $z = M_1/T$, $\varepsilon_{ij}^{(k)} = \varepsilon_k \mathcal{P}_{ij}^{(k)}$ is the CP asymmetry matrix, N_{ij}^{B-L} is the $B - L$ asymmetry matrix, k defines the generation of RHNs(1, 2, 3). Here, $D_k(z) = \frac{z \Gamma_{D_k}(\frac{M_k}{M_1} z)}{\mathcal{H}(M_k)}$ which accounts for the decays of N_k . S_k , $k = 1, 2, 3$ constitutes $\Delta L = 1$ scattering processes involving N_k . W_k represents the washout term due to inverse decays, $\Delta L = 1$ and $\Delta L = 2$ scatterings. The Hubble expansion rate is given by

$$\mathcal{H} \approx \sqrt{\frac{8\pi^3 g_*}{90}} \frac{T^2}{M_{\text{Pl}}} \approx 1.66 \sqrt{g_*} \frac{T^2}{M_{\text{Pl}}}, \quad (19)$$

where, $g_* = g_{\text{SM}} = 106.75$ is the total number of degrees of freedom, $M_{\text{Pl}} = 1.22 \times 10^{19}$ GeV is the Planck mass, and T is the temperature of the thermal bath.

The decay and scattering terms D and S depend on the *effective neutrino mass* defined as

$$\tilde{m}_i = \frac{(m_D^\dagger m_D)_{ii}}{M_i}, \quad (20)$$

which has to be compared with the equilibrium neutrino mass

$$m_* = \frac{16\pi^{5/2} \sqrt{g_*}}{3\sqrt{5}} \frac{v^2}{M_{\text{Pl}}} \approx 1.08 \times 10^{-3} \text{eV}. \quad (21)$$

Then we define the washout parameter as

$$K_i = \frac{\Gamma_i(z = \infty)}{\mathcal{H}(z = 1)} = \frac{\tilde{m}_i}{m_*}. \quad (22)$$

This quantity defines whether or not the decay of N_i is in equilibrium.

The $B - L$ asymmetry obtained in Eq.(18) is then transferred to the baryon asymmetry via EW sphaleron process and can be observed as:

$$\eta_B = \frac{a_{\text{sph}}}{f} N_{B-L}^{\text{final}} \quad (23)$$

where $a_{\text{sph}} = 28/79$ is the fraction of $B - L$ asymmetry transferred to baryon asymmetry and $f = N_{\gamma}^{\text{rec}}/N_{\gamma}^* = 2387/86$ is the dilution factor. Therefore, the correct $B - L$ asymmetry, considering the central value of the observed baryon asymmetry $\eta_B^{\text{obs}} = 6.14 \times 10^{-10}$ is $N_{B-L}^{\text{obs}} \simeq 4.81 \times 10^{-8}$. If we can consider the three ‘‘flavor vectors’’ to be almost parallel to each other ($l_1 || l_2 || l_3$), then we can describe the dynamics by simple Boltzmann equations instead of the density matrix given by

$$\begin{aligned} \frac{dN_{N_1}}{dz} &= -(D_1 + S_1)(N_{N_1} - N_{N_1}^{\text{eq}}), \\ \frac{dN_{N_2}}{dz} &= -(D_2 + S_2)(N_{N_2} - N_{N_2}^{\text{eq}}), \\ \frac{dN_{N_3}}{dz} &= -(D_3 + S_3)(N_{N_3} - N_{N_3}^{\text{eq}}), \\ \frac{dN_{B-L}}{dz} &= -\sum_{i=k}^3 (\varepsilon_k D_k(z)(N_{N_k} - N_{N_k}^{\text{eq}}) + \\ &\quad W_k(z)N_{B-L}(z)), \end{aligned} \quad (24)$$

We can easily get Eq.(24) from Eq.(18) by taking a trace of the whole $B - L$ equation in the condition ($l_1 || l_2 || l_3$). However, if all the ‘‘flavor vectors’’ are parallel to each other, then this will imply that the coefficient matrix $C = \{c_{i\alpha}\}$ is rank 1, and since the coefficient $c_{i\alpha} = \frac{Y_{\alpha i}}{\sqrt{(Y^\dagger Y)_{ii}}}$ at tree level, this means that the Yukawa coupling matrix Y is rank one and will lead to only single non-zero light neutrino mass obtained from seesaw mechanism. But the current neutrino oscillation experiment demands that at least two of the light neutrinos are massive. In order for us to have at least 2 non-zero neutrino masses, at most two out of the three ‘‘flavor vectors’’ can be parallel to each other.

Now, to show the effects of heavy neutrino flavor projection on the final $B - L$ asymmetry, we shall consider two extreme situations.

Case-1: when l_1 and l_2 are parallel to each other.

Case-2: when l_1 and l_2 are orthogonal to each other.

For simplicity, we consider only the effects of decay and inverse decay when solving the DMEs. To simplify the situation, we consider only N_1 and N_2 , whose decay produces the lepton asymmetry. Now we consider N_i decays to $l_i = \frac{Y_{\alpha i}}{\sqrt{(Y^\dagger Y)_{ii}}} l_\alpha$, where $i = 1, 2$ and $\alpha = e, \mu, \tau$.

To show this geometric interpretation, we define the angle between these two ‘‘flavor vectors’’ in the flavor space as

$$\cos \phi_{ij} = \frac{\sum_{\alpha} Y_{\alpha i} Y_{\alpha j}^*}{\sqrt{(Y^\dagger Y)_{ii}} \sqrt{(Y^\dagger Y)_{jj}}}. \quad (25)$$

Fig.4 shows a pictorial representation of the ‘‘flavor vectors’’ l_1 and l_2 and the angle ϕ_{12} between them in the $(l_1, l_1^{\perp(1)}, l_1^{\perp(2)})$ basis in flavor space. Now for case-1, $\cos \phi_{12} \rightarrow 1$ means that l_1 and l_2 are parallel to each other, and for case-2, $\cos \phi_{12} \rightarrow 0$ means that l_1 is orthogonal to l_2 . To illustrate the cases, we consider two benchmark points, BP1 and BP2, as mentioned in Table I. We then compute the projection matrices of the two RHNs for BP1 and BP2. The projection matrices $\mathcal{P}^{(1)}$ and $\mathcal{P}^{(2)}$ are given by Eq.(A1) and Eq.(A2). The 11 component of the projection matrix $\mathcal{P}^{(2)}$ gives the component of l_2 parallel to l_1 . For BP1, $\mathcal{P}_{11}^{(2)} = 0.997$, which shows that l_2 is almost parallel to l_1 . This belongs to our case-1. And for BP2, $\mathcal{P}_{11}^{(2)} = 0.003$ which shows that l_2 is almost orthogonal to l_1 . This belongs to our case-2.

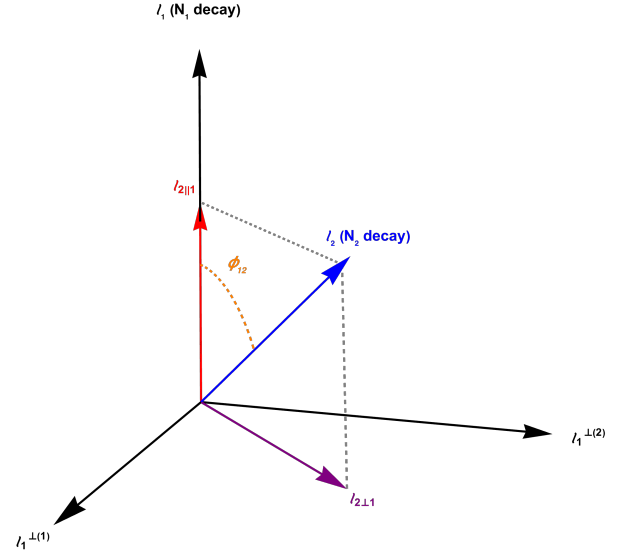


FIG. 4. Figure illustrating the alignment of ‘‘flavor vectors’’ in the $(l_1, l_1^{\perp(1)}, l_1^{\perp(2)})$ basis in flavor space.

In the *left* panel of Fig.5, we show the evolution of the abundances of RHNs and the lepton asymmetries for the BP1 as given in Table I. The Yukawa coupling for this benchmark point is given as

$$Y = \begin{pmatrix} -1.04 \times 10^{-2} + 1.58 \times 10^{-2}i & -7.31 \times 10^{-2} + 9.28 \times 10^{-2}i & -1.05 \times 10^{-2} + 4.40 \times 10^{-1}i \\ -6.02 \times 10^{-4} - 8.61 \times 10^{-2}i & 2.55 \times 10^{-3} - 6.87 \times 10^{-1}i & 2.45 \times 10^{-2} + 4.12 \times 10^{-1}i \\ 2.73 \times 10^{-4} - 9.10 \times 10^{-2}i & -3.82 \times 10^{-3} - 6.66 \times 10^{-1}i & 2.52 \times 10^{-2} - 4.98 \times 10^{-1}i \end{pmatrix}. \quad (26)$$

BPs	$x_1(^{\circ})$	$y_1(^{\circ})$	$x_2(^{\circ})$	$y_2(^{\circ})$	$x_3(^{\circ})$	$y_3(^{\circ})$	M_1 (GeV)	M_2 (GeV)	M_3 (GeV)
BP1	-95.684	-0.0503	-402.789	0.0627	-0.3096	0.7575	2.1×10^{13}	1.05×10^{15}	2.1×10^{15}
BP2	-269.462	-6.307	19.882	-0.01104	-84.7951	-92.705	10^{12}	5×10^{13}	10^{14}

TABLE I. Input parameters for the two benchmark points used in the plots.

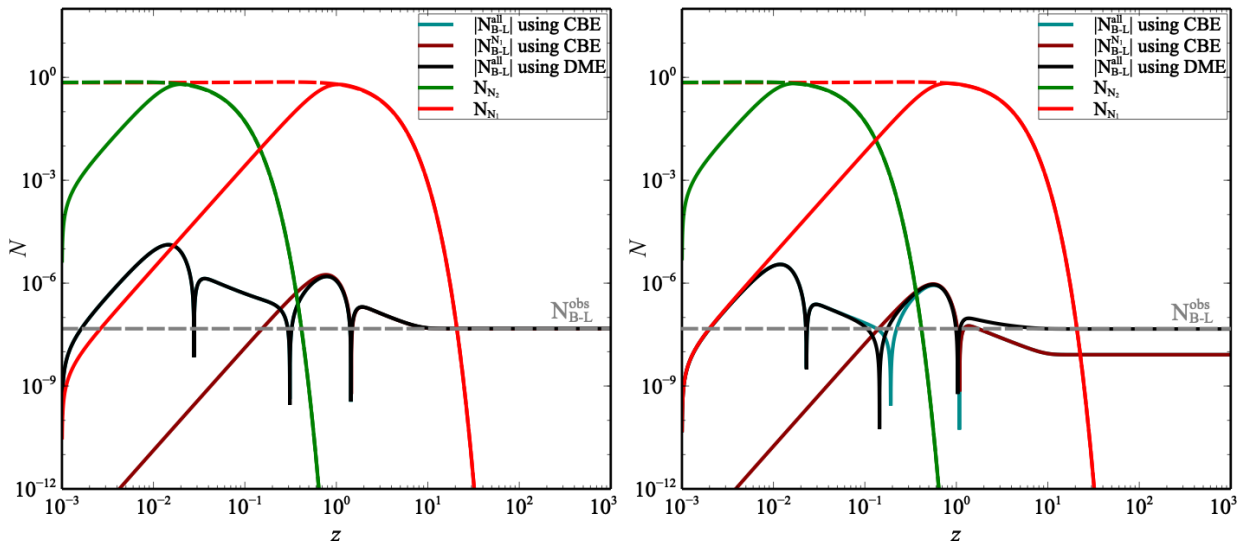


FIG. 5. *Left*: Figure illustrating the effect of “flavor vector” in parallel orientation ($\cos \phi_{12} \rightarrow 1$) (Yukawa coupling texture) on the final $B - L$ asymmetry. (BP-1: $K_1 = 21.62$ and $K_2 = 25.06$). *Right*: figure illustrating the effect of “flavor vector” in orthogonal orientation ($\cos \phi_{12} \rightarrow 0$) (Yukawa coupling texture) on the final $B - L$ asymmetry. (BP-2: $K_1 = 54.50$ and $K_2 = 45.15$).

Here, both RHNs N_1 and N_2 are in the strong washout regime. Here, the black curve denotes the $B - L$ asymmetry produced by both N_1 and N_2 using the DM formalism (*i.e.*, Eq.(18)), the dark-red curve denotes the $B - L$ asymmetry produced by the decay of N_1 alone, and the dark-cyan curve represents the $B - L$ asymmetry produced by both N_1 and N_2 using the Classical Boltzmann equation (CBE) (*i.e.*, Eq.(24)). The red and green curves denote the comoving number densities of N_1 and N_2 , respectively. The dashed red and blue curves denote the respective comoving equilibrium number densities. And finally the gray dashed line represents the correct $B - L$ asymmetry. In this plot, we observe that there is no

difference in the final asymmetry produced by N_1 alone compared to that produced by both N_1 and N_2 using both approaches. Here, all the RHNs are in the strong washout regime, so this result is expected. This says that since the “flavor vectors” are parallel to each other, any asymmetry produced by heavier RHN (N_2) is fully washed out by the inverse decays of the lighter RHN N_1 . This also shows that when $l_1 \parallel l_2$, then the DME Eq.(18) collapses to the CBE Eq.(24)

On the other hand, in the *right* panel of Fig.5, we show the evolution of the abundances and asymmetries for the BP2 as given in Table I. The Yukawa coupling matrix for BP2 is given as

$$Y = \begin{pmatrix} 8.23 \times 10^{-4} - 2.10 \times 10^{-2}i & 2.33 \times 10^{-2} - 7.56 \times 10^{-2}i & -2.11 \times 10^{-1} - 1.71 \times 10^{-2}i \\ 1.04 \times 10^{-3} - 3.66 \times 10^{-2}i & -2.79 \times 10^{-4} + 1.35 \times 10^{-1}i & -2.87 \times 10^{-1} - 1.55 \times 10^{-2}i \\ -3.13 \times 10^{-3} + 1.15 \times 10^{-2}i & -4.30 \times 10^{-3} + 2.35 \times 10^{-1}i & 1.73 \times 10^{-1} + 2.97 \times 10^{-2}i \end{pmatrix}. \quad (27)$$

In this case, all the RHNs are in the strong washout regime. The color code for the curves in the plot is same as the previous one. Here we observe that, within the classical Boltzmann treatment, the $B - L$ asymmetry obtained from N_1 alone is indistinguishable from that

obtained when both N_1 and N_2 are included. However, within the DM framework, there is a clear difference in the final $B - L$ asymmetry produced by only N_1 in comparison to the asymmetry produced by both N_1 and N_2 . This shows that in this case, there is some memory left of

the asymmetry produced by the heavier RHN N_2 . The physical essence of this benchmark point is that the ‘‘flavor vectors’’ are almost orthogonal to each other, which means that the asymmetry produced by N_2 is almost fully protected from the inverse-decay washout effects of N_1 , and therefore the final asymmetry remaining is basically the sum of the asymmetries produced by N_1 and N_2 . This essence is captured by the density-matrix formalism and therefore differs from the classical Boltzmann approach. Therefore, we see that this case goes against the conventional assumption that the lightest RHN fully washes out any asymmetry previously produced, and thus shows the effect of the Yukawa coupling texture (projection effect) on the final $B - L$ asymmetry.

A. Washout Regime Analysis

As previously defined in Eq.(22) we have

$$K_i = \frac{\tilde{m}_i M_i^2 / 8\pi v^2}{1.66\sqrt{g_s} M_i^2 / M_{\text{Pl}}} = \frac{\tilde{m}_i}{1.0697 \times 10^{-3} \text{ eV}}, \quad (28)$$

where $\tilde{m}_i = \frac{v^2(Y_\nu^\dagger Y_\nu)_{ii}}{2M_i}$. If $K_i < 1$ ($\tilde{m}_i < 1.0697 \times 10^{-3}$ eV), then the i^{th} RHN is in the weak washout regime. On the other hand, if $K_i > 1$ ($\tilde{m}_i > 1.0697 \times 10^{-3}$ eV) then the i^{th} RHN is in the strong washout regime. Using Eq.(8) we can write

$$\begin{aligned} \tilde{m}_i &= \frac{1}{M_i} [(U^* D_{\sqrt{m}} R^T D_{\sqrt{M}})^\dagger (U^* D_{\sqrt{m}} R^T D_{\sqrt{M}})]_{ii}, \\ &= \frac{1}{M_i} [(D_{\sqrt{M}} R^* D_{\sqrt{m}} U^T) (U^* D_{\sqrt{m}} R^T D_{\sqrt{M}})]_{ii}, \\ &= \frac{1}{M_i} [D_{\sqrt{M}} R^* D_m R^T D_{\sqrt{M}}]_{ii}. \end{aligned} \quad (29)$$

By using the generalized rotation matrix, R given by Eq.(10) and putting it in the above Eq.(29) we get

$$\begin{aligned} \tilde{m}_1 &= |\cos \theta_1 \cos \theta_2|^2 m_1 + |\cos \theta_1 \sin \theta_2 \sin \theta_3 \\ &\quad - \sin \theta_1 \cos \theta_3|^2 m_2 + |\cos \theta_1 \sin \theta_2 \cos \theta_3 \\ &\quad + \sin \theta_1 \sin \theta_3|^2 m_3, \\ \tilde{m}_2 &= |\sin \theta_1 \cos \theta_2|^2 m_1 + |\sin \theta_1 \sin \theta_2 \sin \theta_3 \\ &\quad + \cos \theta_1 \cos \theta_3|^2 m_2 + |\sin \theta_1 \sin \theta_2 \cos \theta_3 \\ &\quad - \cos \theta_2 \cos \theta_3|^2 m_3, \\ \tilde{m}_3 &= |\sin \theta_2|^2 m_1 + |\cos \theta_2 \sin \theta_3|^2 m_2 \\ &\quad + |\cos \theta_2 \cos \theta_3|^2 m_3. \end{aligned} \quad (30)$$

So from the above equation we notice that condition for washout regime, either $K_i < 1$ ($\tilde{m}_i < 1.0697 \times 10^{-3}$ eV) or $K_i > 1$ ($\tilde{m}_i > 1.0697 \times 10^{-3}$ eV) depends on the absolute mass of the light neutrinos which can be obtained from the neutrino oscillation data. Now we ask the question, for a given set of light neutrino masses (m_1, m_2, m_3), how many RHNs can be in the weak washout regime ($\tilde{m}_i < 1.0697 \times 10^{-3}$ eV $\forall i$). This question can be answered from a simple analysis using the method of contradiction as given below. For normal mass ordering (NO)

of the light active neutrinos, we set $m_1 \rightarrow 0$ for simplicity, and then $m_2 = \sqrt{|\Delta m_{21}^2|}$ and $m_3 = \sqrt{\Delta m_{31}^2}$. Let us assume all RHNs to be in weak washout regime ($\tilde{m}_i < 1.0697 \times 10^{-3}$ eV $\forall i$). Now assuming $\theta_2 = \theta_3 = \frac{\pi}{2}$ in Eq.(30) we get $\tilde{m}_3 \rightarrow 0$ and

$$\begin{aligned} |\cos \theta_1|^2 m_2 + |\sin \theta_1|^2 m_3 &< 1.0697 \times 10^{-3} \text{ eV}, \\ |\sin \theta_1|^2 m_2 + |\cos \theta_1|^2 m_3 &< 1.0697 \times 10^{-3} \text{ eV}. \end{aligned} \quad (31)$$

From the above inequalities, we get

$$m_2 + m_3 < 2.1394 \times 10^{-3} \text{ eV}. \quad (32)$$

Similarly, in the case of inverse mass ordering (IO) of the light active neutrinos, we set $m_3 \rightarrow 0$, then $m_1 = \sqrt{|\Delta m_{31}^2|}$ and $m_2 = \sqrt{|\Delta m_{31}^2| + \Delta m_{21}^2}$. Now if we take all the RHNs to be in weak washout regime ($\tilde{m}_i < 1.0697 \times 10^{-3}$ eV $\forall i$) and $\theta_2 = \theta_3 = \frac{\pi}{2}$, we get $\tilde{m}_3 \rightarrow 0$ and

$$\begin{aligned} |\cos \theta_1|^2 m_1 + |\sin \theta_1|^2 m_2 &< 1.0697 \times 10^{-3} \text{ eV}, \\ |\sin \theta_1|^2 m_1 + |\cos \theta_1|^2 m_2 &< 1.0697 \times 10^{-3} \text{ eV}, \end{aligned} \quad (33)$$

which gives,

$$m_1 + m_2 < 2.1394 \times 10^{-3} \text{ eV}. \quad (34)$$

From Eqs.32 and 34, we see that the inequalities cannot be satisfied by the low-energy neutrino oscillation data[3, 42]. This implies that our initial assumption that all three RHNs are simultaneously in the weak washout regime is incorrect. On the other hand, from Eq.(32) we can see that the condition $m_2 + m_3 > 2.1394 \times 10^{-3}$ eV ($m_1 + m_2 > 2.1394 \times 10^{-3}$ eV) can be satisfied by the low-energy neutrino oscillation data for NO (IO). So the above analysis shows that when N_3 is in the weak washout regime, both N_1 and N_2 must be in the strong washout regime. This same exercise can be repeated by setting $\tilde{m}_1, \tilde{m}_2 \rightarrow 0$, which shows that for a given set of m_1, m_2, m_3 at most one of the RHNs can be in the weak washout regime[38].

Although in the above analysis we fixed the value of $\theta_2, \theta_3 = \pi/2$, it can be generalized by considering arbitrary complex values of $\theta_i \forall i$ as shown in Fig.6. For simplicity, we choose the lightest neutrino mass m_1 (m_3) to be zero for NO (IO). We illustrate the results, (i) for normal ordering in the plane of $K_3 - K_2$ with K_1 in color code as shown in Fig.6 (left) and (ii) for inverse ordering in the plane of $K_2 - K_1$ with K_3 in the color code as shown in Fig.6 (right). For analysis purpose, we divide Fig.6 (left) into four zones, (I) $K_2, K_3 < 1$, (II) $K_2 < 1, K_3 > 1$, (III) $K_2, K_3 > 1$ and (IV) $K_2 > 1, K_3 < 1$. In the zone (I), no points indicate that N_2 and N_3 simultaneously being in the weak washout regime is not possible. In zone (II), when N_2 is in the weak washout regime, N_1 and N_3 are in the strong washout regime. In zone (III), when N_2 and N_3 are in a strong washout regime, then we have two possibilities: either N_1 is in a strong washout regime (colored points), or it is in a weak washout regime

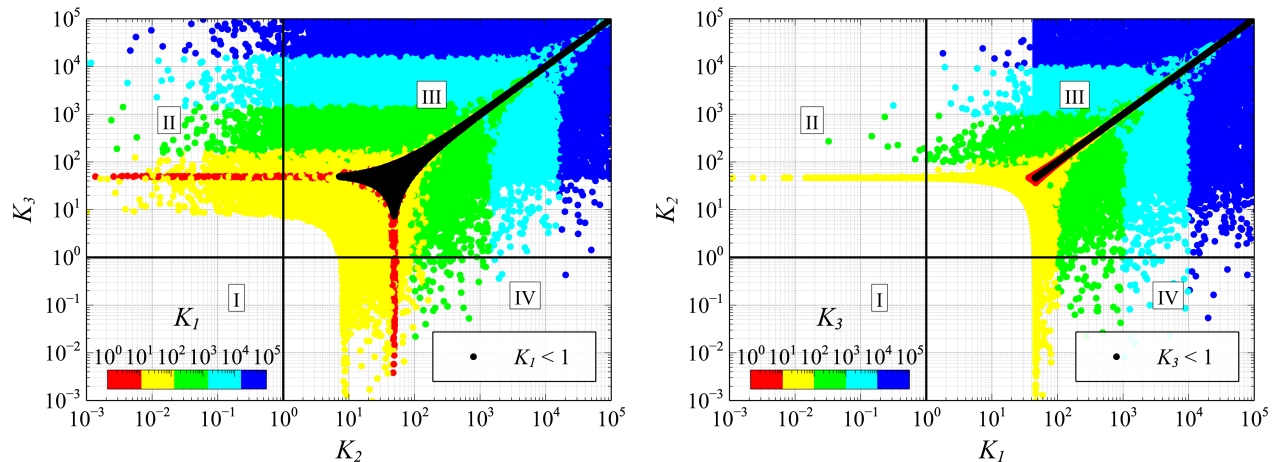


FIG. 6. Plot illustrating the constraints between K_1 , K_2 , and K_3 and thereby showing that at most only one of the three *RHNs* can be in weak washout regime in the case of normal ordering (*left*), and inverse ordering (*right*).

(black points). Finally, in zone (IV), when N_3 is in the weak washout regime, then N_1 and N_2 are in the strong washout regime. The same analysis is valid for inverse ordering as shown in the Fig.6(*right*). This validates the analytical proof we showed above.

IV. DYNAMICAL EVOLUTION OF $B - L$ ASYMMETRY IN THERMAL LEPTOGENESIS

Based on the discussion in section III A, we concluded that at most one of the *RHNs* can be in a weak wash-out regime. This divides our analysis into four cases: (1) all three *RHNs* are in a strong washout regime, (2) N_1 is in a weak washout regime, (3) N_2 is in a weak washout regime, and (4) N_3 is in a weak washout regime.

As discussed in the literature [6–12], in the type-I seesaw framework, N_1 is the only d.o.f. which is responsible for thermal leptogenesis. This is because any asymmetry produced by $N_{2,3}$ is presumed to be washed out by the lepton number-violating interactions of N_1 . However, when we take projection effects into account, we saw that the asymmetry produced by $N_{2,3}$ may not be washed out fully even if N_1 is in the strong washout regime. To capture this effect, we define the parameter δ as

$$\delta = \frac{N_{B-L}^{\text{all}} - N_{B-L}^1}{N_{B-L}^1} \times 100\%. \quad (35)$$

where, N_{B-L}^1 denotes the final $B - L$ asymmetry when only N_1 contribution to $B - L$ asymmetry is under consideration, and N_{B-L}^{all} denotes the final $B - L$ asymmetry when all N_1, N_2, N_3 simultaneously contribute. From Eq.(35), $\delta \rightarrow 0$ implies that solving the density matrix equation 18 considering all the *RHNs* is equivalent to solving Eq.(24) by considering only N_1 contribution. In other words, $\delta \rightarrow 0$ implies N_1 is the only d.o.f, and one

can neglect the contribution from $N_{2,3}$ safely. Any non-zero values of δ imply a *memory* effect on the final $B - L$ asymmetry.

To generate the $B - L$ asymmetry dynamically, we solve the DMEs (Eq.(18)), considering decay, inverse decay, and scatterings. It is worth noting that scatterings are dominant in the early times, while decay dominates in late times. We analyze each washout scenario individually in the plane of mass ratios M_2/M_1 and M_3/M_1 , while keeping the CI parameters fixed as given in tab.II. We focus only on the region of parameter space where the density matrix equation (DME) yields correct N_{B-L} , and corresponding to the observed η_B . In our numerical setup, we record all the points lying in the range: $5.1 \times 10^{-8} \gtrsim N_{B-L} \gtrsim 4.3 \times 10^{-8}$. With this in mind, we analyze all the above-mentioned cases.

1. All *RHNs* are in strong washout regime

In this case, we have taken all the *RHNs* to be in the strong washout regime by fixing the C.I. angles as given in the Table II (case-1(a)). We vary the two mass ratios M_2/M_1 and M_3/M_1 and check the memory effect. The left panel of Fig.7 shows the values of δ (colored points) in the plane of M_3/M_1 and M_2/M_1 for a typical values of the washout parameters $K_1 = 42.60$, $K_2 = 13.77$, $K_3 = 12.81$. And we have also fixed the mass of N_1 as $M_1 = 10^{12}\text{GeV}$. Fixing the Casas-Ibarra parameters also fixes the projection matrices ($\mathcal{P}^{(1)}$, $\mathcal{P}^{(2)}$, $\mathcal{P}^{(3)}$) in the $(\ell_1, \ell_1^{\perp(1)}, \ell_1^{\perp(2)})$ basis, as given in Eq.(A3). From Eq.(A3), we obtain $\mathcal{P}_{11}^{(2)} = 0.20$ and $\mathcal{P}_{11}^{(3)} = 0.63$. This implies that a significant fraction of the asymmetry produced from N_2 decay is protected from the N_1 washout, whereas the asymmetry generated from N_3 decay is more strongly affected by the N_1 washout. Consequently, N_2 decay is expected to provide the domi-

Cases	$x_1(^{\circ})$	$y_1(^{\circ})$	$x_2(^{\circ})$	$y_2(^{\circ})$	$x_3(^{\circ})$	$y_3(^{\circ})$	M_1 (GeV)
Case-1 (a)	-374.803	-34.2302	250.481	-8.19379	4.42873	2.18086	10^{12}
Case-1 (b)	42.079	-7.9681	-3.818×10^{-2}	3.877×10^{-2}	-443.96	1.9254×10^{-3}	10^{12}
Case-2	-44.898	-4.7806	-8.43×10^{-4}	1.66×10^{-1}	-8.23×10^{-2}	5.71×10^{-1}	10^{12}
Case-3	-4.62×10^{-2}	1.35×10^{-3}	448.112	-13.045	274.443	-1.78×10^{-2}	10^{12}
Case-4	-95.632	-2.616×10^{-1}	8.097×10^{-3}	1.1025	280.247	6.2784	3×10^{12}

TABLE II. Input parameters for the four washout regimes.

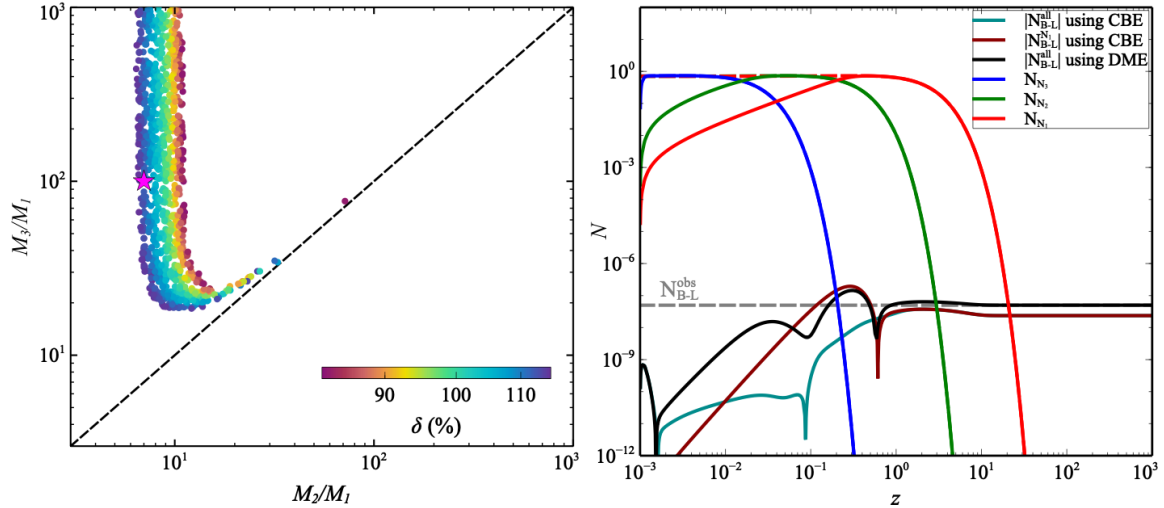


FIG. 7. [Left:] Allowed parameter space in the plane M_3/M_1 vs M_2/M_1 when all the RHNs are in strong washout regime. The color code depicts the δ values representing the *memory* effect. [Right:] Cosmological evolution of comoving number densities of RHNs and $B - L$ asymmetries for the magenta star point when all RHNs are in the strong washout regime.

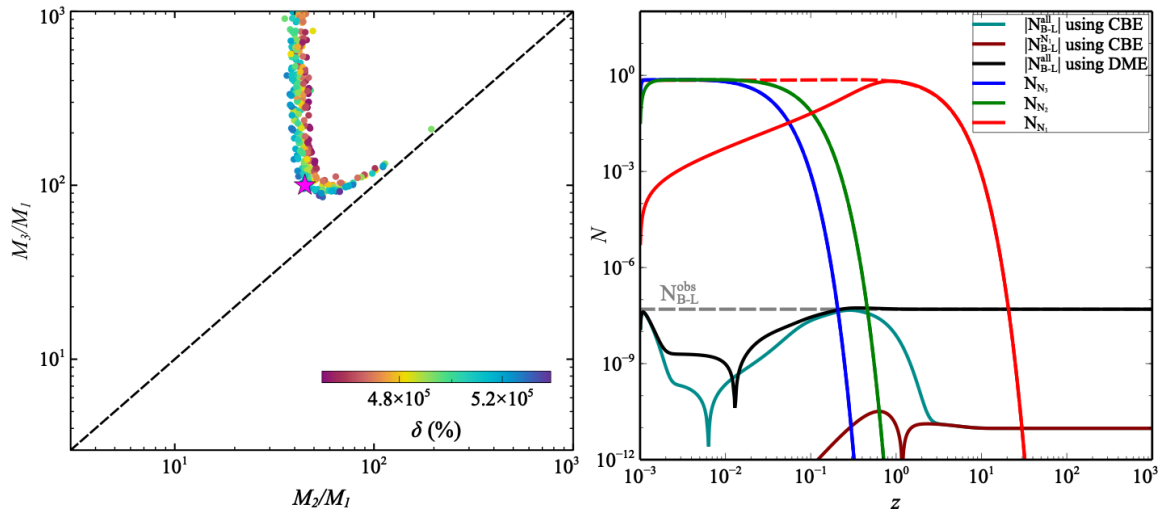


FIG. 8. [Left:] Allowed parameter space in the plane M_3/M_1 vs M_2/M_1 when all the RHNs are in strong washout regime. The color code depicts the δ values representing the *memory* effect. [Right:] Cosmological evolution of comoving number densities of RHNs and $B - L$ asymmetries for the magenta star point when all RHNs are in the strong washout regime.

nant contribution to the final $B - L$ asymmetry. Figure 7 (left) shows the parameter space that yield the correct $B - L$ asymmetry within the density matrix formalism. It also highlights a significant deviation due to the memory effect (70 – 130%). Due to the mass hierar-

chy among the RHNs ($M_3 > M_2 > M_1$), all points appear above the diagonal dashed-black line. Since a large fraction of the asymmetry generated from N_3 decay is washed out by N_1 , the allowed parameter space mainly depends on M_2/M_1 . We observe that the memory effect

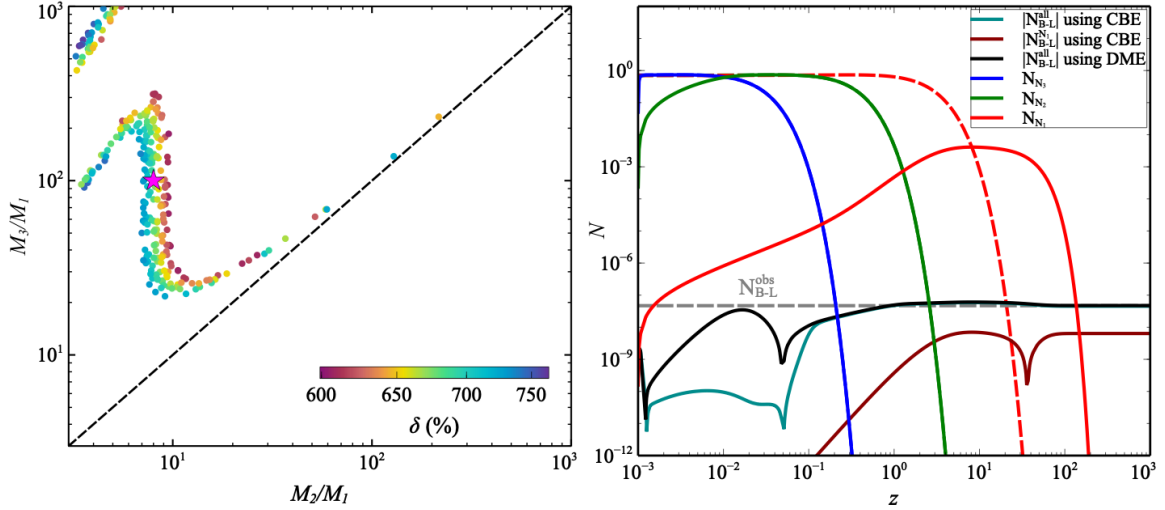


FIG. 9. [Left:] Allowed parameter space in the plane M_3/M_1 vs M_2/M_1 when N_1 is in weak washout regime. The color code depicts the δ values representing the *memory* effect. [Right:] Cosmological evolution of comoving number densities of RHNs and $B - L$ asymmetries for the magenta star point when N_1 is in the weak washout regime.

decreases as M_2/M_1 increases. As a result, the region with $M_2/M_1 \lesssim 6$ leads to an overproduction of asymmetry, while the region with $M_2/M_1 \gtrsim 11$ becomes underabundant. However, this trend does not always hold. When $M_3 \gtrsim M_2$, the two heavier RHNs decay nearly simultaneously and generate a larger asymmetry. Consequently, even parameter points with $M_2/M_1 > 11$ can

yield the correct $B - L$ asymmetry in this regime.

The right panel of Fig. 7 illustrates a benchmark point with mass ratios $M_2/M_1 = 7$ and $M_3/M_1 = 100$, which is shown as a magenta star in Fig. 7(left). This benchmark corresponds to a typical hierarchical spectrum (*i.e.* $M_3 > M_2 > M_1$) with the Yukawa coupling matrix as:

$$Y = \begin{pmatrix} (-2.59 \times 10^{-3} + 4.85 \times 10^{-3}i) & (8.95 \times 10^{-3} + 2.98 \times 10^{-2}i) & (-7.72 \times 10^{-2} + 5.44 \times 10^{-2}i) \\ (-1.08 \times 10^{-3} - 2.65 \times 10^{-2}i) & (-1.01 \times 10^{-2} + 3.44 \times 10^{-2}i) & (-4.06 \times 10^{-2} - 6.57 \times 10^{-2}i) \\ (-1.62 \times 10^{-3} - 2.77 \times 10^{-2}i) & (-2.27 \times 10^{-2} - 2.53 \times 10^{-2}i) & (8.72 \times 10^{-2} - 1.51 \times 10^{-1}i) \end{pmatrix} \quad (36)$$

The evolution of the RHN abundances N_1 , N_2 , and N_3 is shown in solid red, green, and blue, respectively. The $B - L$ asymmetry generated by N_1 alone is indicated by the dark-red curve, while the solid black curve shows the asymmetry obtained by including all three RHNs within the density-matrix framework. For comparison, the dark-cyan curve corresponds to the classical Boltzmann treatment considering all three RHNs contributing to the final $B - L$ asymmetry without projection effects. The gray-dashed line represents the correct $B - L$ asymmetry. In this case, the large Yukawa couplings also result in rapid inverse decays and scatterings, which quickly wash out the asymmetries generated by N_2 and N_3 . This is clearly visible in the classical Boltzmann solution shown by the dark-cyan curve. However, due to the projection effects, a large portion of the asymmetry produced by heavier RHNs is not subjected to the washout effects. This is clearly visible in the black curve (obtained by solving Eq.(18)), which retains a large asymmetry, illustrating the sizable memory effect.

The parameter space we got in the Fig.7 (left) is not unique and is completely dependent on the Yukawa coupling matrix and thereby on the CI parameters chosen. In order to demonstrate this, we consider another example of all strong washout regime where the DME gives correct relic in a different parameter space. The CI parameter chosen for this example is given in Table II (Case-1 (b)). Fig 8 (left) shows a new parameter space in the plane of M_2/M_1 and M_3/M_1 for correct $B - L$ asymmetry generated from density matrix approach with $K_1 = 8.00$, $K_2 = 22.01$, and $K_3 = 26.77$. Here, the parameter space for correct relic has been shifted to $48 \gtrsim M_2/M_1 \gtrsim 38$ with very small dependence on N_3 . An interesting thing to notice here is that the memory effect in this case is much larger compared to the previous case. The reason mainly lies in the projection effects. From Eq.(A4), we can see that $\mathcal{P}_{11}^{(2)} = 0.003$ and $\mathcal{P}_{11}^{(3)} = 0.002$, which means the decays of both the RHNs N_2 and N_3 are completely perpendicular to the N_1 decay and therefore almost all of the asymmetry produced by heavier generation is pro-

tected which gives such a large memory effect. In order to show this nature in detail, we have also shown a benchmark plot, Fig. 7 (right) with the mass splitting

$$Y = \begin{pmatrix} (1.31 \times 10^{-6} - 9.22 \times 10^{-3}i) & (1.04 \times 10^{-2} - 2.07 \times 10^{-2}i) & (2.78 \times 10^{-2} - 4.21 \times 10^{-2}i) \\ (-5.23 \times 10^{-4} - 1.10 \times 10^{-2}i) & (1.87 \times 10^{-2} + 1.31 \times 10^{-1}i) & (-2.74 \times 10^{-2} + 1.99 \times 10^{-1}i) \\ (-5.56 \times 10^{-4} + 8.71 \times 10^{-3}i) & (2.12 \times 10^{-2} + 1.28 \times 10^{-1}i) & (-2.68 \times 10^{-2} + 2.26 \times 10^{-1}i) \end{pmatrix} \quad (37)$$

The color code is same as the previous benchmark plot. Here, we see that the heavier generations produce very large asymmetries which is visible from both black and darkcyan curve but only when we consider the projection effects can we get the correct $B-L$ asymmetry even when N_1 is heavily underabundant.

2. N_1 is in weak washout regime

Now, we consider the scenario where N_1 is in the weak washout regime. As indicated in Fig. 6, if N_1 is in the weak washout regime, then the other two RHNs, N_2 and N_3 , must necessarily be in the strong washout regime. To do this, we fix the C.I. parameters as given in Table II (case-2). This gives us the washout parameters as $K_1 = 1.22 \times 10^{-3}$, $K_2 = 27.79$, and $K_3 = 27.93$. We also fix the mass of N_1 as $M_1 = 10^{12}$ GeV. Since we fix the C.I. parameter, this fixes the projection matrices, and in this case, they are given as Eq.(A5). From Eq.(A5), we see that $\mathcal{P}_{11}^{(2)} = 0.059$ and $\mathcal{P}_{11}^{(3)} = 0.707$, meaning that the decays of N_2 is almost completely perpendicu-

$M_2/M_1 = 45$ and $M_3/M_1 = 100$ as shown by the magenta star in Fig. 7 (left). The corresponding Yukawa coupling matrix is given as

lar but decays of N_3 are almost completely parallel to N_1 decays. That is the asymmetry produced by N_3 is largely affected by N_1 washout effects, but N_2 being almost perpendicular largely affects the final asymmetry. The resulting value of δ is shown in Fig.9 (left), in the plane of $M_3/M_1 - M_2/M_1$.

As N_1 is in weak washout regime, the Yukawa coupling of N_1 is small. Thus, the pre-existing asymmetry left by N_2 and N_3 persist in the final result, and we therefore see a large *memory* effect. Due to the mass hierarchy, all points lie above the diagonal dashed-black line. We see that as mass of N_2 increases memory effect decreases. Therefore the region $M_2/M_1 < 7$ is mostly overabundant, and region where $M_2/M_1 > 10$ is mostly underabundant.

Now to explain the scenario more clearly, we choose a benchmark point as shown with a star in the left panel of Fig.9. We show the evolution of the asymmetries in the right panel of Fig.9 and the color code remains the same as in the right panel of Fig.7. This BP corresponds to $M_2/M_1 = 9$ and $M_3/M_1 = 100$ with the Yukawa coupling matrix as

$$Y = \begin{pmatrix} (-7.76 \times 10^{-5} - 3.93 \times 10^{-6}i) & (-5.74 \times 10^{-3} + 2.84 \times 10^{-2}i) & (1.43 \times 10^{-2} + 2.73 \times 10^{-2}i) \\ (-1.91 \times 10^{-4} - 1.12 \times 10^{-5}i) & (7.48 \times 10^{-3} - 3.31 \times 10^{-2}i) & (1.33 \times 10^{-2} + 2.75 \times 10^{-1}i) \\ (1.64 \times 10^{-6} + 1.76 \times 10^{-5}i) & (4.52 \times 10^{-3} - 7.64 \times 10^{-2}i) & (2.63 \times 10^{-2} + 1.46 \times 10^{-1}i) \end{pmatrix}. \quad (38)$$

Here, the asymmetry is effectively produced by N_2 as any asymmetry produced by N_3 is washed out by N_2 and N_1 washout effects, and the asymmetry generated by N_2 survives with and without the projection effects as N_1 is in weak washout regime.

3. N_2 is in weak washout regime

We now move to the case where N_2 is in the weak washout regime, while N_1 and N_3 remain in the strong washout regime. We consider a typical case by taking the C.I. parameters as given in Table II (case-3). This gives us the washout parameters $K_1 = 39.712$, $K_2 = 4.75 \times 10^{-2}$, $K_3 = 10.98$, and the mass of N_1 is fixed as $M_1 =$

10^{12} GeV. As we fix the C.I. parameters, the projection matrices also get fixed, which are given in this case by Eq.(A6). From Eq.(A6), we see that $\mathcal{P}_{11}^{(2)} = 0.008$ and $\mathcal{P}_{11}^{(3)} = 0.310$, meaning that a large amount of asymmetry produced by N_2 and N_3 is protected from the N_1 washout effects. Only about one-third of the asymmetry produced by N_3 is subjected to N_1 washout.

Figure 10 (left) shows the variation of the values of δ in the plane of M_2/M_1 and M_3/M_1 corresponding to correct $B-L$ asymmetry points. From Fig. 10 (left), we see that almost all the points in the plot show a large memory effect. That is, the asymmetries produced by N_2 and N_3 contribute significantly to the final $B-L$ asymmetry.

In this case both N_2 and N_3 affects the final $B-L$

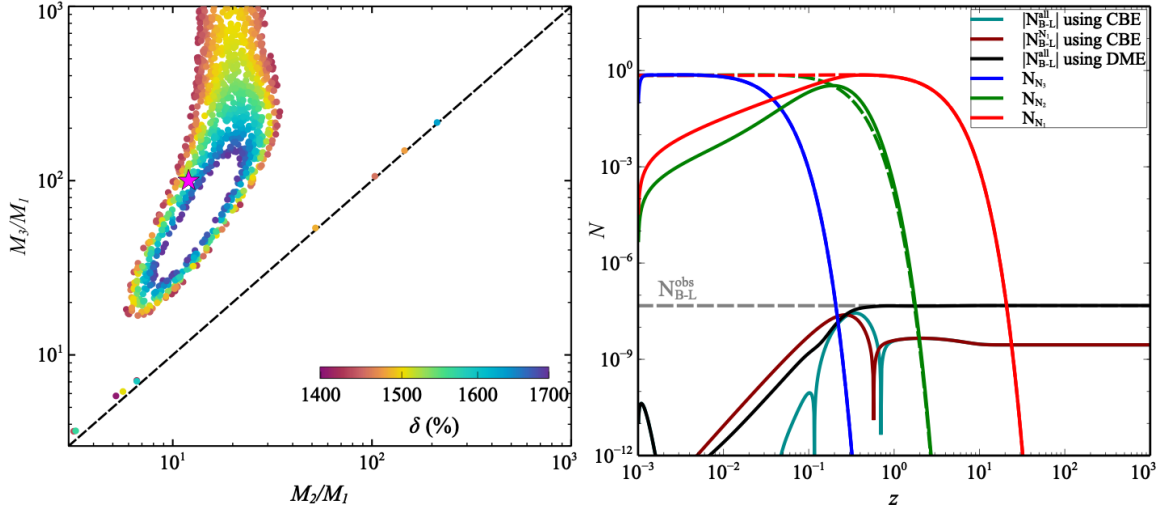


FIG. 10. [Left:] Allowed parameter space in the plane M_3/M_1 vs M_2/M_1 when N_2 is in weak washout regime. The color code depicts the δ values representing the *memory* effect. [Right:] Cosmological evolution of comoving number densities of RHNs and $B - L$ asymmetries for the magenta star point when N_2 is in the weak washout regime.

asymmetry. As the asymmetry produced by both the RHNs are almost perpendicular we can see that the region for correct $B - L$ asymmetry increases almost linearly with N_2 and N_3 mass. But for very large N_3 mass compared to N_2 , its effect almost ceases. This is due to the N_3 asymmetry being washed out by scattering processes. Another point to note is that the parameter space shown in the Fig. 10 (left), has two regions disconnected from each other. The points outside are underabundant regions whereas the small hole with no points are over-

abundant region. This does not apply to the points near the diagonal as here the mass of N_2 and N_3 are close and this causes increase in CP asymmetry (resonance region) and they produce correct asymmetry simultaneously.

To explain this more we have shown a case study in the right panel of Fig. 10 by choosing a benchmark point (marked by the magenta star in the left panel of Fig. 10). For this point, we take $M_2/M_1 = 12$ and $M_3/M_1 = 100$, and the color code is the same as in the previous plots with the Yukawa coupling matrix for this case as:

$$Y = \begin{pmatrix} (5.38 \times 10^{-3} - 5.60 \times 10^{-3}i) & (5.34 \times 10^{-6} + 2.46 \times 10^{-3}i) & (1.36 \times 10^{-2} + 1.01 \times 10^{-1}i) \\ (2.72 \times 10^{-3} + 2.78 \times 10^{-2}i) & (1.63 \times 10^{-4} + 2.93 \times 10^{-3}i) & (-5.73 \times 10^{-2} + 1.22 \times 10^{-1}i) \\ (-1.81 \times 10^{-3} + 3.02 \times 10^{-2}i) & (1.53 \times 10^{-4} - 2.33 \times 10^{-3}i) & (-6.24 \times 10^{-2} - 7.99 \times 10^{-2}i) \end{pmatrix}. \quad (39)$$

Here, the asymmetry produced by N_3 remains protected from $N_{1,2}$ washout effects and is further increased by the asymmetry produced by N_2 . This results in a large memory effect and the final value lying in the range of correct $B - L$ asymmetry even when N_1 is underabundant.

4. N_3 is in weak washout regime

Now we turn to the final possibility, i.e., when N_3 is in the weak washout regime. The C.I. parameters are fixed as given in Table II (case-4). Here, $K_1 = 7.95$, $K_2 = 46.44$ and $K_3 = 7.99 \times 10^{-1}$. We fix the mass of N_1 to be $M_1 = 3 \times 10^{12} \text{GeV}$. From Eq.(A7), we get $\mathcal{P}_{11}^{(2)} = 0.004$ and $\mathcal{P}_{11}^{(3)} = 0.412$, which tell us that the decay of N_2 is completely orthogonal to N_1 , whereas the decay of N_3 has both parallel and perpendicular components to

N_1 . We show points corresponding to the correct $B - L$ asymmetry and their memory effect in terms of mass ratios M_2/M_1 vs M_3/M_1 in the left panel of Fig. 11. We observe that all points lie very close to the diagonal line, indicating that the masses of N_2 and N_3 are very close to each other. The region above these points corresponds to underabundance. In this scenario, N_2 is in a relatively strong washout regime, which suppresses both the asymmetry generated by N_3 and its own produced asymmetry. Consequently, the heavier generation can significantly impact the final $B - L$ asymmetry only when $M_3 \gtrsim M_2$, where it can generate a sufficiently large memory effect to yield the correct $B - L$ asymmetry.

This behavior is further explained in Fig. 11(right), where we consider the benchmark mass ratios $M_2/M_1 = 42$ and $M_3/M_1 = 46$, ensuring that the mass ratios are relatively close. The Yukawa coupling matrix for this

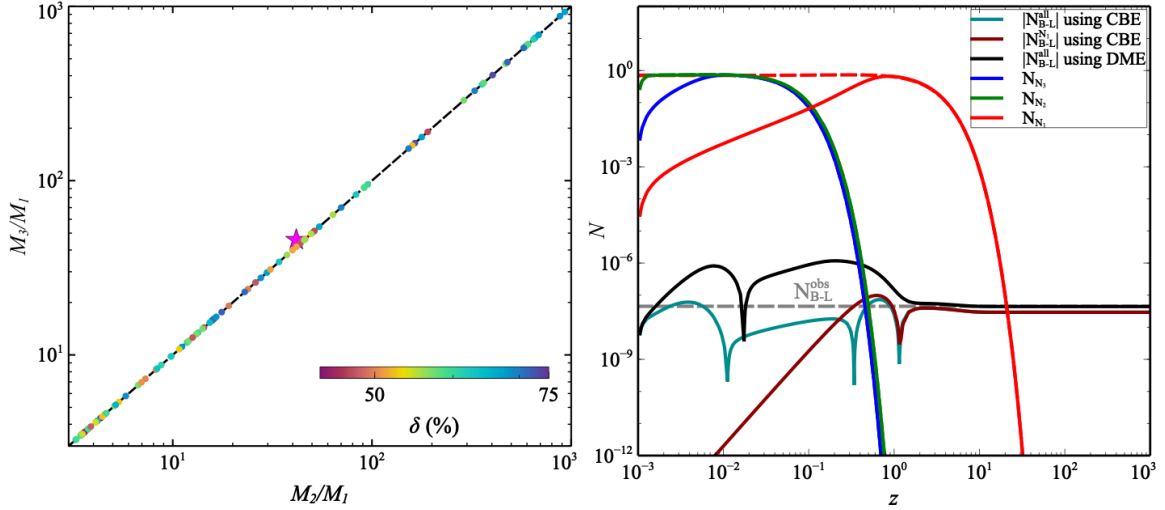


FIG. 11. [Left:] Allowed parameter space in the plane M_3/M_1 vs M_2/M_1 when N_3 is in weak washout regime. The color code depicts the δ values representing the *memory* effect. [Right:] Cosmological evolution of comoving number densities of RHNs and $B - L$ asymmetries for the magenta star point when N_3 is in the weak washout regime.

benchmark point is given as

$$Y = \begin{pmatrix} (-1.42 \times 10^{-4} - 1.58 \times 10^{-2}i) & (-3.26 \times 10^{-2} + 5.54 \times 10^{-2}i) & (-1.54 \times 10^{-2} + 2.51 \times 10^{-2}i) \\ (-2.16 \times 10^{-3} - 1.89 \times 10^{-2}i) & (3.52 \times 10^{-3} - 3.10 \times 10^{-1}i) & (-1.11 \times 10^{-2} - 8.03 \times 10^{-3}i) \\ (-1.60 \times 10^{-3} + 1.51 \times 10^{-2}i) & (-3.24 \times 10^{-3} - 3.25 \times 10^{-1}i) & (1.35 \times 10^{-2} - 5.13 \times 10^{-2}i) \end{pmatrix}. \quad (40)$$

The color code remains the same as in previous cases. Since the masses of N_2 and N_3 are close, the asymmetry generated by N_3 is large and is not significantly affected by the washout effects of N_2 . Finally, due to projection effects, this asymmetry is protected and adds to the asymmetry produced by N_1 , resulting in the final $B - L$ asymmetry.

V. REVISITING PREVIOUS ANALYTICAL RESULTS WITH FULL NUMERICAL SOLUTIONS

We now turn to compare the analytical solution of DME of earlier works [12, 32–40] to our numerical solution of the DME. In the limit of two RHNs, the analytical solution of Eq.(18) is given as [33]

$$N_{\text{ana}}^{B-L} = \varepsilon_1 \kappa(K_1) + (e^{-\frac{3\pi}{8}K_1} p_{12} + 1 - p_{12}) \varepsilon_2 \kappa(K_2) \quad (41)$$

where $\kappa(K_1)$ is the final efficiency factor given as

$$\kappa(x) = \frac{2}{xz_B(x)} \left(1 - e^{-\frac{1}{2}xz_B(x)} \right) \quad (42)$$

where,

$$z_{B_i} \approx 2 + 4K_i^{0.13} e^{-2.5/K_i}. \quad (43)$$

To quantify the validity of the analytical approximation to the density matrix equations (DMEs), we define the relative deviation parameter

$$\delta' \equiv \frac{N_{\text{num}}^{B-L} - N_{\text{ana}}^{B-L}}{N_{\text{ana}}^{B-L}} \times 100\%, \quad (44)$$

where N_{num}^{B-L} , N_{ana}^{B-L} denote the lepton asymmetry obtained from the full numerical solution of the DMEs and from the analytical approximation, respectively. In Fig. 12, we present the parameter space yielding the correct baryon asymmetry in the plane of M_3/M_1 vs M_2/M_1 for $\theta = 5.317 \times 10^{-4} - i1.685 \times 10^{-2}$ and $M_1 = 4 \times 10^{12}$ GeV. The color coding represents the magnitude of δ' . We observe that for large $M_2/M_1 \simeq 20 - 30$, analytical estimation matches very accurately with the numerical solution. On the other hand, for small $M_2/M_1 \simeq 3 - 10$, the deviation typically lies in the range $\delta' \gtrsim 10 - 50\%$, indicating that the analytical approximation systematically underestimates the baryon asymmetry compared to the full numerical DME solution. This behavior is physically expected. When the mass hierarchy is small, N_2 remains thermally populated during the epoch in which N_1 dynamics are relevant. In that case, the off-diagonal entries of the density matrix contribute appreciably to the final asymmetry. For larger hierarchies, N_2 has already decayed or is Boltzmann suppressed well before

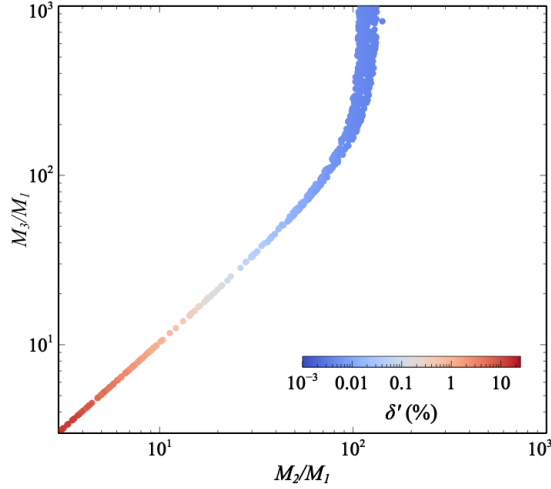


FIG. 12. Correct lepton asymmetry parameter space in the plane of $M_3/M_1 - M_2/M_1$ with $M_1 = 4 \times 10^{12}$ GeV and $\theta = 5.317 \times 10^{-4} - 1.685 \times 10^{-2} * i$. The color code denotes δ' . See main text for details.

N_1 becomes active, and the two-flavored analytical approximation matches the full numerical solution. This demonstrates the necessity of numerically accounting for projection effects in DME solutions, particularly in moderate mass hierarchies.

VI. IMPORTANCE OF PROJECTION EFFECTS IN PROBING LEPTOGENESIS WITH NEUTRINOLESS DOUBLE BETA DECAY

Neutrinoless double beta ($0\nu\beta\beta$) decay constitutes one of the most sensitive probes of the Majorana nature of neutrinos and provides complementary information on the absolute neutrino mass scale. The quantity relevant for $0\nu\beta\beta$ decay experiments is the effective neutrino mass, defined as

$$m_{\beta\beta} = m_1 \cos^2 \theta_{12} \cos^2 \theta_{13} e^{2i\phi_1} + m_2 \sin^2 \theta_{12} \cos^2 \theta_{13} e^{2i\phi_2} + m_3 \sin^2 \theta_{13}. \quad (45)$$

Here, m_1 denotes the lightest SM neutrino mass. Assuming normal ordering, the remaining neutrino masses are given by $m_2 = \sqrt{\Delta m_{21}^2 + m_1^2}$ and $m_3 = \sqrt{\Delta m_{31}^2 + m_1^2}$, while ϕ_1 and ϕ_2 represent the Majorana phases. The lightest neutrino mass m_1 thus emerges as a common parameter governing both leptogenesis and neutrinoless double beta ($0\nu\beta\beta$) decay. In this work, we investigate the possibility of constraining leptogenesis through current and future sensitivities of $0\nu\beta\beta$ decay experiments.³ Figure 13 shows the correlation between the

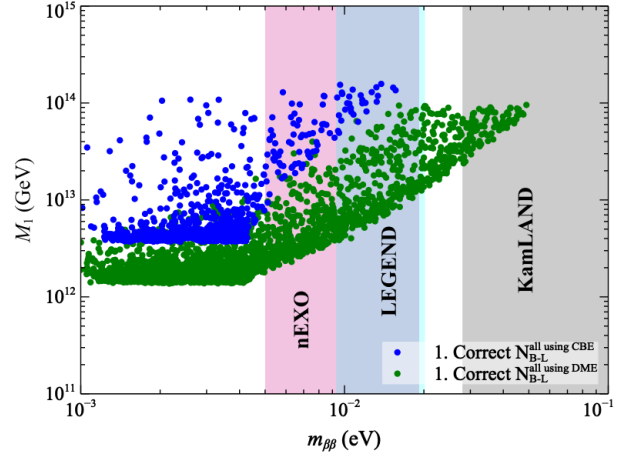


FIG. 13. The lightest RHN mass as a function of effective neutrino mass. Here we fixed $\theta = 3.38582 + 1.50555 \times 10^{-4}i$ radians, $M_2/M_1 = 25$ and $M_3/M_1 = 100$. The neutrino oscillation data are varied within 3σ range with the Majorana phases varied within $[0, 2\pi]$. The KamLAND-Zen exclusion limit is shown as a gray-shaded region. The future sensitivities of nEXO and LEGEND are shown in pink and cyan shaded regions, respectively.

lightest right-handed neutrino mass M_1 and the effective neutrino mass $m_{\beta\beta}$ relevant for neutrinoless double beta decay in three different scenarios. Here, the blue points correspond to the parameter choices that yield the observed baryon asymmetry when all the RHNs are considered for the asymmetry production with CBE, while the green points represent solutions obtained using the density matrix equations, which consistently account for projection effects. Here, we fix the CI rotation angle to $\theta = 3.38582 + i1.50555 \times 10^{-4}$, taking hierarchical heavy neutrinos with mass ratios $M_2/M_1 = 25$ and $M_3/M_1 = 100$, and vary the neutrino oscillation parameters in 3σ range with Majorana phases in the range $[0, 2\pi]$ [44]. The shaded regions indicate current and future sensitivities of neutrinoless double beta decay experiments: the present KamLAND-Zen [45] exclusion bound (gray), and the projected sensitivities of nEXO [46] (pink) and LEGEND [47] (cyan). A clear separation is observed between the regions preferred by the Boltzmann and density matrix treatments. In particular, the density matrix approach allows successful leptogenesis for significantly lower values of M_1 at fixed $m_{\beta\beta}$, reflecting the impact of projection effects neglected in the classical approximation. Remarkably, a substantial portion of the parameter space compatible with density-matrix leptogenesis falls within the reach of upcoming neutrinoless double beta decay experiments, highlighting a non-trivial interplay between the dynamics of leptogenesis and low energy lepton number violating observables. The reason for this is that for this choice of parameters, ℓ_2 and ℓ_1 are not parallel to each other and hence have significant projection effects. These effects reduce the required mass scale of the lightest right-handed neutrino, thereby allowing

³ For simplicity, and in order to clearly illustrate the impact of projection effects, we ignore the contribution of N_3 to the final lepton asymmetry.

the correct baryon asymmetry to be achieved for larger values of m_1 while keeping the Yukawa couplings within the perturbative regime. Such a parameter space is not accessible within the classical Boltzmann approach. This distinction is reflected in the predictions for neutrinoless double beta decay.

VII. CONCLUSIONS

In the standard treatment of thermal leptogenesis with hierarchical right-handed neutrinos, it is commonly assumed that the final $B - L$ asymmetry is solely determined by the dynamics of the lightest state, N_1 , since any pre-existing asymmetry generated by N_2 or N_3 is expected to be completely washed out. While several earlier studies have demonstrated that this assumption can fail in scenarios of N_2 -dominated leptogenesis, such analyses typically rely on classical Boltzmann equations and specific washout hierarchies. In this work, we have shown that a qualitatively different, more general phenomenon emerges when flavor projection effects are treated consistently within the density-matrix formalism. We find that the asymmetries generated by N_2 and N_3 are typically not fully aligned with the flavor direction washed out by N_1 , leading to a continuous, quantifiable memory effect, even in parameter regions where N_1 interactions remain active. This effect is therefore distinct from the conventional notion of N_2 -dominated leptogenesis. By combining the density-matrix evolution with constraints from low-energy neutrino oscillation data, we further show that only one RHN can be in the weak-washout regime, which naturally organizes the parameter space into four

distinct dynamical regimes. In all cases, we find that the memory effect enhances the surviving asymmetry compared to classical Boltzmann treatments that consider either only N_1 decay or sequential decays of all RHNs. Our results demonstrate that the standard reduction of hierarchical leptogenesis to an effective single-RHN description can fail even outside the usual N_2 -dominated regime, highlighting the importance of density matrix effects in accurately determining the final baryon asymmetry. We also show that when the mass hierarchy between N_1 and N_2 is less than 15-20, the analytical approximation underestimates the baryon asymmetry compared to the full numerical solution of density matrix equations.

We find that incorporating projection effects into the density-matrix treatment significantly enlarges the viable parameter space, extending it into the sensitivity range of neutrinoless double beta decay experiments. As a result, these experiments can probe a substantial portion of the parameter space relevant for both the seesaw mechanism and leptogenesis, thereby providing meaningful and complementary constraints on the underlying neutrino mass-generation scale and the dynamics responsible for the baryon asymmetry of the Universe.

ACKNOWLEDGMENTS

P.K.P. would like to acknowledge the Ministry of Education, Government of India, for providing financial support for his research via the Prime Minister's Research Fellowship (PMRF) scheme. The work of N.S. is supported by the Department of Atomic Energy - Board of Research in Nuclear Sciences, Government of India (Ref. Number: 58/14/15/2021-BRNS/37220). We thank the anonymous Referee(s) of Physical Review D for their constructive comments, which improved the manuscript.

Appendix A: Projection Matrices for different cases:

Using the Eq.(16) and Eq.(17), we can write down the projection matrices for all three right-handed neutrinos in the $(\ell_1, \ell_1^{(1)}, \ell_1^{(2)})$ basis.

1. Projection matrices for section III

Here, we present the projection matrices obtained for the parameters given in Table I. The following projection matrices are used when ℓ_1 and ℓ_2 are parallel to each other, demonstrated in Fig.5(left).

$$\mathcal{P}^{(1)} = \begin{pmatrix} 1 & 0 & 0 \\ 0 & 0 & 0 \\ 0 & 0 & 0 \end{pmatrix}; \mathcal{P}^{(2)} = \begin{pmatrix} 0.997 & -0.011 - 0.038i & 0.033 - 0.011i \\ -0.011 + 0.038i & 0.002 & 0.000 + 0.001i \\ 0.033 + 0.011i & 0.000 - 0.001i & 0.001 \end{pmatrix}. \quad (\text{A1})$$

The following projection matrices are used when ℓ_1 and ℓ_2 are orthogonal to each other, demonstrated in Fig.5(right).

$$\mathcal{P}^{(1)} = \begin{pmatrix} 1 & 0 & 0 \\ 0 & 0 & 0 \\ 0 & 0 & 0 \end{pmatrix}; \mathcal{P}^{(2)} = \begin{pmatrix} 0.003 & -0.008 + 0.045i & -0.025 - 0.0003i \\ -0.008 - 0.045i & 0.770 & 0.067 + 0.413i \\ -0.025 + 0.0003i & 0.067 - 0.413i & 0.227 \end{pmatrix} \quad (\text{A2})$$

2. Projection matrices for section IV

Here, we present the projection matrices obtained for each washout regime using the parameters given in Table II.

a. All Strong regime

Case-1 (a):

$$\begin{aligned} \mathcal{P}^{(1)} &= \begin{pmatrix} 1 & 0 & 0 \\ 0 & 0 & 0 \\ 0 & 0 & 0 \end{pmatrix}; \mathcal{P}^{(2)} = \begin{pmatrix} 0.201 & 0.300 + 0.032i & -0.026 + 0.262i \\ 0.300 - 0.032i & 0.453 & 0.003 + 0.396i \\ -0.026 - 0.262i & 0.003 - 0.396i & 0.346 \end{pmatrix}; \\ \mathcal{P}^{(3)} &= \begin{pmatrix} 0.633 & 0.253 + 0.260i & -0.226 + 0.223i \\ 0.253 - 0.260i & 0.208 & 0.001 + 0.182i \\ -0.226 - 0.223i & 0.001 - 0.182i & 0.159 \end{pmatrix}. \end{aligned} \quad (\text{A3})$$

Case-1 (b):

$$\begin{aligned} \mathcal{P}^{(1)} &= \begin{pmatrix} 1 & 0 & 0 \\ 0 & 0 & 0 \\ 0 & 0 & 0 \end{pmatrix}; \mathcal{P}^{(2)} = \begin{pmatrix} 0.003 & -0.013 + 0.040i & -0.026 - 0.005i \\ -0.013 - 0.040i & 0.709 & 0.046 + 0.450i \\ -0.026 + 0.005i & 0.046 - 0.450i & 0.288 \end{pmatrix}; \\ \mathcal{P}^{(3)} &= \begin{pmatrix} 0.002 & -0.011 - 0.031i & 0.019 - 0.009i \\ -0.011 + 0.031i & 0.710 & 0.046 + 0.450i \\ 0.019 + 0.009i & 0.046 - 0.450i & 0.288 \end{pmatrix}. \end{aligned} \quad (\text{A4})$$

b. N_1 in weak washout regime

$$\begin{aligned} \mathcal{P}^{(1)} &= \begin{pmatrix} 1 & 0 & 0 \\ 0 & 0 & 0 \\ 0 & 0 & 0 \end{pmatrix}; \mathcal{P}^{(2)} = \begin{pmatrix} 0.059 & -0.194 - 0.081i & 0.107 + 0.023i \\ -0.194 + 0.081i & 0.741 & -0.379 + 0.069i \\ 0.107 - 0.023i & -0.379 - 0.069i & 0.200 \end{pmatrix}; \\ \mathcal{P}^{(3)} &= \begin{pmatrix} 0.707 & -0.403 + 0.020i & 0.204 - 0.048i \\ -0.403 - 0.020i & 0.230 & -0.118 + 0.022i \\ 0.204 + 0.048i & -0.118 - 0.022i & 0.062 \end{pmatrix}. \end{aligned} \quad (\text{A5})$$

c. N_2 in weak washout regime

$$\begin{aligned} \mathcal{P}^{(1)} &= \begin{pmatrix} 1 & 0 & 0 \\ 0 & 0 & 0 \\ 0 & 0 & 0 \end{pmatrix}; \mathcal{P}^{(2)} = \begin{pmatrix} 0.008 & -0.065 + 0.002i & -0.004 + 0.058i \\ -0.065 - 0.002i & 0.555 & 0.046 - 0.490i \\ -0.004 - 0.058i & 0.046 + 0.490i & 0.438 \end{pmatrix}; \\ \mathcal{P}^{(3)} &= \begin{pmatrix} 0.310 & -0.331 + 0.101i & 0.062 + 0.301i \\ -0.331 - 0.101i & 0.386 & 0.032 - 0.341i \\ 0.062 - 0.301i & 0.032 + 0.341i & 0.305 \end{pmatrix}. \end{aligned} \quad (\text{A6})$$

d. N_3 in weak washout regime

$$\mathcal{P}^{(1)} = \begin{pmatrix} 1 & 0 & 0 \\ 0 & 0 & 0 \\ 0 & 0 & 0 \end{pmatrix}; \mathcal{P}^{(2)} = \begin{pmatrix} 0.004 & -0.050 + 0.007i & -0.006 - 0.032i \\ -0.050 - 0.007i & 0.707 & 0.023 + 0.452i \\ -0.006 + 0.032i & 0.023 - 0.452i & 0.289 \end{pmatrix};$$

$$\mathcal{P}^{(3)} = \begin{pmatrix} 0.412 & 0.185 - 0.371i & 0.243 + 0.106i \\ 0.185 + 0.371i & 0.417 & 0.014 + 0.267i \\ 0.243 - 0.106i & 0.014 - 0.267i & 0.171 \end{pmatrix}. \quad (\text{A7})$$

-
- [1] N. Aghanim *et al.* (Planck), Planck 2018 results. VI. Cosmological parameters, *Astron. Astrophys.* **641**, A6 (2020), [Erratum: *Astron. Astrophys.* 652, C4 (2021)], [arXiv:1807.06209 \[astro-ph.CO\]](#).
- [2] B. Fields and S. Sarkar, Big Bang Nucleosynthesis, (2004), [arXiv:astro-ph/0406663](#).
- [3] S. Navas *et al.* (Particle Data Group), Review of particle physics, *Phys. Rev. D* **110**, 030001 (2024).
- [4] R. H. Cyburt, B. D. Fields, K. A. Olive, and E. Skillman, New BBN limits on physics beyond the standard model from ${}^4\text{He}$, *Astropart. Phys.* **23**, 313 (2005), [arXiv:astro-ph/0408033](#).
- [5] G. Steigman, Primordial nucleosynthesis: successes and challenges, *Int. J. Mod. Phys. E* **15**, 1 (2006), [arXiv:astro-ph/0511534](#).
- [6] M. Fukugita and T. Yanagida, Baryogenesis Without Grand Unification, *Phys. Lett. B* **174**, 45 (1986).
- [7] M. A. Luty, Baryogenesis via leptogenesis, *Phys. Rev. D* **45**, 455 (1992).
- [8] R. N. Mohapatra and X. Zhang, Electroweak baryogenesis in left-right-symmetric models, *Phys. Rev. D* **46**, 5331 (1992).
- [9] M. Flanz, E. A. Paschos, and U. Sarkar, Baryogenesis from a lepton asymmetric universe, *Phys. Lett. B* **345**, 248 (1995), [Erratum: *Phys. Lett. B* 384, 487–487 (1996), Erratum: *Phys. Lett. B* 382, 447–447 (1996)], [arXiv:hep-ph/9411366](#).
- [10] S. Davidson, E. Nardi, and Y. Nir, Leptogenesis, *Phys. Rept.* **466**, 105 (2008), [arXiv:0802.2962 \[hep-ph\]](#).
- [11] W. Buchmüller, P. Di Bari, and M. Plumacher, Leptogenesis for pedestrians, *Annals Phys.* **315**, 305 (2005), [arXiv:hep-ph/0401240](#).
- [12] R. Barbieri, P. Creminelli, A. Strumia, and N. Tetradis, Baryogenesis through leptogenesis, *Nucl. Phys. B* **575**, 61 (2000), [arXiv:hep-ph/9911315](#).
- [13] A. Pilaftsis and T. E. J. Underwood, Resonant leptogenesis, *Nucl. Phys. B* **692**, 303 (2004), [arXiv:hep-ph/0309342](#).
- [14] A. Pilaftsis and T. E. J. Underwood, Electroweak-scale resonant leptogenesis, *Phys. Rev. D* **72**, 113001 (2005), [arXiv:hep-ph/0506107](#).
- [15] E. Nardi, Y. Nir, E. Roulet, and J. Racker, The Importance of flavor in leptogenesis, *JHEP* **01**, 164, [arXiv:hep-ph/0601084](#).
- [16] P. F. de Salas, D. V. Forero, C. A. Ternes, M. Tortola, and J. W. F. Valle, Status of neutrino oscillations 2018: 3σ hint for normal mass ordering and improved CP sensitivity, *Phys. Lett. B* **782**, 633 (2018), [arXiv:1708.01186 \[hep-ph\]](#).
- [17] K. Abe *et al.* (T2K), Measurements of neutrino oscillation in appearance and disappearance channels by the T2K experiment with 6.6×10^{20} protons on target, *Phys. Rev. D* **91**, 072010 (2015), [arXiv:1502.01550 \[hep-ex\]](#).
- [18] M. G. Aartsen *et al.* (IceCube), The IceCube Neutrino Observatory - Contributions to ICRC 2015 Part II: Atmospheric and Astrophysical Diffuse Neutrino Searches of All Flavors, in *34th International Cosmic Ray Conference* (2015) [arXiv:1510.05223 \[astro-ph.HE\]](#).
- [19] J. N. Bahcall and C. Pena-Garay, Solar models and solar neutrino oscillations, *New J. Phys.* **6**, 63 (2004), [arXiv:hep-ph/0404061](#).
- [20] S. Fukuda *et al.* (Super-Kamiokande), Constraints on neutrino oscillations using 1258 days of Super-Kamiokande solar neutrino data, *Phys. Rev. Lett.* **86**, 5656 (2001), [arXiv:hep-ex/0103033](#).
- [21] K. Eguchi *et al.* (KamLAND), First results from KamLAND: Evidence for reactor anti-neutrino disappearance, *Phys. Rev. Lett.* **90**, 021802 (2003), [arXiv:hep-ex/0212021](#).
- [22] P. Minkowski, $\mu \rightarrow e\gamma$ at a Rate of One Out of 10^9 Muon Decays?, *Phys. Lett. B* **67**, 421 (1977).
- [23] M. Gell-Mann, P. Ramond, and R. Slansky, Complex Spinors and Unified Theories, *Conf. Proc. C* **790927**, 315 (1979), [arXiv:1306.4669 \[hep-th\]](#).
- [24] O. Sawada and A. Sugamoto, eds., *Proceedings: Workshop on the Unified Theories and the Baryon Number in the Universe: Tsukuba, Japan, February 13-14, 1979* (Natl. Lab. High Energy Phys., Tsukuba, Japan, 1979).
- [25] R. N. Mohapatra and G. Senjanović, Neutrino mass and spontaneous parity nonconservation, *Phys. Rev. Lett.* **44**, 912 (1980).
- [26] J. Schechter and J. W. F. Valle, Neutrino Masses in $SU(2) \times U(1)$ Theories, *Phys. Rev. D* **22**, 2227 (1980).
- [27] J. W. F. Valle and J. C. Romao, *Neutrinos in high energy and astroparticle physics*, Physics textbook (Wiley-VCH, Weinheim, 2015).
- [28] A. D. Sakharov, Violation of CP Invariance, C asymmetry, and baryon asymmetry of the universe, *Pisma Zh. Eksp. Teor. Fiz.* **5**, 32 (1967).
- [29] V. A. Kuzmin, V. A. Rubakov, and M. E. Shaposhnikov, On the Anomalous Electroweak Baryon Number Non-conservation in the Early Universe, *Phys. Lett. B* **155**, 36 (1985).
- [30] M. Plumacher, Baryogenesis and lepton number violation, *Z. Phys. C* **74**, 549 (1997), [arXiv:hep-ph/9604229](#).
- [31] O. Vives, Flavor dependence of CP asymmetries and

- thermal leptogenesis with strong right-handed neutrino mass hierarchy, *Phys. Rev. D* **73**, 073006 (2006), [arXiv:hep-ph/0512160](#).
- [32] G. Engelhard, Y. Grossman, E. Nardi, and Y. Nir, The Importance of N_2 leptogenesis, *Phys. Rev. Lett.* **99**, 081802 (2007), [arXiv:hep-ph/0612187](#).
- [33] S. Blanchet, P. Di Bari, D. A. Jones, and L. Marzola, Leptogenesis with heavy neutrino flavours: from density matrix to Boltzmann equations, *JCAP* **01**, 041, [arXiv:1112.4528 \[hep-ph\]](#).
- [34] E. Bertuzzo, P. Di Bari, and L. Marzola, The problem of the initial conditions in flavoured leptogenesis and the tauon N_2 -dominated scenario, *Nucl. Phys. B* **849**, 521 (2011), [arXiv:1007.1641 \[hep-ph\]](#).
- [35] S. Antusch, P. Di Bari, D. A. Jones, and S. F. King, Leptogenesis in the Two Right-Handed Neutrino Model Revisited, *Phys. Rev. D* **86**, 023516 (2012), [arXiv:1107.6002 \[hep-ph\]](#).
- [36] K. Moffat, S. Pascoli, S. T. Petcov, H. Schulz, and J. Turner, Three-flavored nonresonant leptogenesis at intermediate scales, *Phys. Rev. D* **98**, 015036 (2018), [arXiv:1804.05066 \[hep-ph\]](#).
- [37] P. Di Bari, On the origin of matter in the Universe, *Prog. Part. Nucl. Phys.* **122**, 103913 (2022), [arXiv:2107.13750 \[hep-ph\]](#).
- [38] P. Di Bari, Seesaw geometry and leptogenesis, *Nucl. Phys. B* **727**, 318 (2005), [arXiv:hep-ph/0502082](#).
- [39] F. Hahn-Woernle, Wash-Out in $N(2)$ -dominated leptogenesis, *JCAP* **08**, 029, [arXiv:0912.1787 \[hep-ph\]](#).
- [40] M. Re Fiorentin, The N_2 -dominated scenario of leptogenesis, *PoS CORFU2014*, 121 (2015).
- [41] J. A. Casas and A. Ibarra, Oscillating neutrinos and $\mu \rightarrow e, \gamma$, *Nucl. Phys. B* **618**, 171 (2001), [arXiv:hep-ph/0103065](#).
- [42] P. F. de Salas, D. V. Forero, S. Gariazzo, P. Martínez-Miravé, O. Mena, C. A. Ternes, M. Tórtola, and J. W. F. Valle, 2020 global reassessment of the neutrino oscillation picture, *JHEP* **02**, 071, [arXiv:2006.11237 \[hep-ph\]](#).
- [43] S. Davidson and A. Ibarra, A Lower bound on the right-handed neutrino mass from leptogenesis, *Phys. Lett. B* **535**, 25 (2002), [arXiv:hep-ph/0202239](#).
- [44] I. Esteban, M. C. Gonzalez-Garcia, M. Maltoni, I. Martinez-Soler, J. P. Pinheiro, and T. Schwetz, NuFit-6.0: updated global analysis of three-flavor neutrino oscillations, *JHEP* **12**, 216, [arXiv:2410.05380 \[hep-ph\]](#).
- [45] S. Abe *et al.* (KamLAND-Zen), Search for Majorana Neutrinos with the Complete KamLAND-Zen Dataset, *Phys. Rev. Lett.* **135**, 262501 (2025), [arXiv:2406.11438 \[hep-ex\]](#).
- [46] G. Adhikari *et al.* (nEXO), nEXO: neutrinoless double beta decay search beyond 10^{28} year half-life sensitivity, *J. Phys. G* **49**, 015104 (2022), [arXiv:2106.16243 \[nucl-ex\]](#).
- [47] N. Abgrall *et al.* (LEGEND), The Large Enriched Germanium Experiment for Neutrinoless $\beta\beta$ Decay: LEGEND-1000 Preconceptual Design Report, (2021), [arXiv:2107.11462 \[physics.ins-det\]](#).